Series 01 Aerodynamics 11

# Design of a Michelson Interferometer for Quantitative Refraction Index Profile Measurements

*J.L.M. Nijholt*

Delft University Press

# Design of a Michelson Interferometer for Quantitative Refraction Index Profile Measurements

# Series 01: Aerodynamics 11

# Design of a Michelson Interferometer for Quantitative Refraction Index Profile Measurements

*J.L.M. Nijholt*


Delft University Press / 1998

*Published and distributed by:*

Delft University Press
Mekelweg 4
2628 CD Delft
The Netherlands
Telephone +31 (0)15 278 32 54
Fax +31 (0)15 278 16 61
e-mail: DUP@DUP.TUDelft.NL

*by order of:*

Faculty of Aerospace Engineering
Delft University of Technology
Kluyverweg 1
P.O. Box 5058
2600 GB Delft
The Netherlands
Telephone +31 (0)15 278 14 55
Fax +31 (0)15 278 18 22
e-mail: Secretariaat@LR.TUDelft.NL
website: http://www.lr.tudelft.nl/

*Cover:* Aerospace Design Studio, 66.5 x 45.5 cm, by:
Fer Hakkaart, Dullenbakkersteeg 3, 2312 HP Leiden, The Netherlands
Tel. +31 (0)71 512 67 25

90-407-1574-2



Printed in The Netherlands

# Contents

# Summary

This report describes the theoretical design of a three camera Michelson interferometer set-up for quantitative refractive index measurements. Although a two camera system is easier to align and less expensive, a three camera interferometer is preferred because the expected measuring accuracy is much better. Here analytical expressions are found for the calculation of the required alignment accuracy of the interferometer's components: three CCD-cameras (six degrees of freedom each), a quarter wave plate (one degree of freedom) and a polariser (one degree of freedom). Also the required accuracy in the normalization of the intensity levels on the CCD-cameras is calculated. If the maximum phase gradient after imaging on the CCD-cameras is $10^5$ rad/m and the average modulus of the phase error is required to be less than 9% of $2\pi$, the required alignment and normalization accuracies are:

CCD-cameras:
- translation perpendicular to beam propagation direction: 0.5$\mu$m
- translation parallel to beam propagation direction: 2.4m
- rotation about axis perpendicular to beam propagation direction: 1.1°
- rotation about optical axis of the beam: 0.01°
- normalization factor two cameras: 13%
- normalization factor one camera: 9%

rotation quarter wave plate: 1.7°
rotation polariser: 3.5°

The error of 9% of $2\pi$ in the average modulus of the phase error excludes errors due to light refraction in the examined medium.

# 1. Introduction

Until now there exists almost no convenient way for real-time quantitative refractive index measurements, especially when the refractive index profile is varying both temporally and spatially. However, there are many applications for an instrument which is capable of measuring refractive index profiles in real time. In most applications, the refractive index profile in the examined transparent medium is caused by an existing density profile. Scientific areas in which such an instrument can be applied, are:

- Compressible gas flow measurements.
- Heat transfer research. The density profile is caused by locally heating of a transparent medium.
- Research on mixing of two or more fluids of different density.
- Combustion research. The density profiles are now caused by all three former effects: compressibility, local heating and mixing.
- Optical research. The exact (time dependent) refractive index of optical components can be measured before they are used in optical set-ups.

Interferometry has shown to be a convenient tool for refractive index profile measurements. It is often applied, especially holographic interferometry. The disadvantage of holographic interferometry, however, is that it is inconvenient for real-time measurements and repetitive measurements. That is why a new interferometer has been designed. The work described in this report is concerned with the development of an electro-optical interferometer for real-time refractive index profile measurements.

The first application in mind is quantitative measurement of refractive index profiles in compressible wind tunnel flows. The main objective is to provide a tool featuring density turbulence diagnostics in two dimensional flow. In relation to other methods for flow measurement, interferometry has several advantages. Unlike hot wire methods and pressure measurement methods, the flow is not disturbed by a probe during the experiments. Unlike laser-Doppler velocimetry and particle image velocimetry, there is no necessity of adding particles to the flow. Unlike Schlieren methods, the absolute refractive index is measured and not its gradient.

The new real-time interferometer is based on a Michelson interferometer set-up. An alternative set-up would be a Mach-Zehnder interferometer set-up. The most essential difference between these two set-ups is the number of passages of the test beam through the test section. In a Mach-Zehnder interferometer the test beam passes the test section only once. In a Michelson interferometer, however, the test beam passes the test section twice: once in forward direction and after reflection by a flat mirror once in backward direction. The main advantage of the Michelson interferometer when compared to the Mach-Zehnder interferometer is the fact that it is relatively easy to install around large objects like a wind tunnel. Contrary to the Mach-Zehnder interferometer, all optical elements can be positioned on one side of the tunnel. Only one mirror has to be installed on the other side. This implies that a Michelson interferometer set-up can lead to a

relatively compact and transportable measuring system. However, due to the double passage of the test beam through the test section there exist two disadvantages when a Michelson interferometer is compared to a Mach-Zehnder interferometer. These disadvantages are:

- A reference object in the test section cannot be imaged sharply in the interference pattern.
- Disturbance of the interference pattern due to refraction in the test section will be larger.

Refractive index profile measurements by interferometry require an analysis of two or more interference patterns which are shifted in phase to each other. In holographic interferometers and other interferometers for steady refractive index profile measurements, these patterns are imaged on the same CCD-camera one by one. In the new real-time interferometer, however, the interference patterns have to be analysed at the same time. This requires that each interference pattern has to be imaged on a separate camera. This implies that the interferometer has to be equipped with two or more cameras.
The exact number of cameras in the new interferometer is determined by the required measuring accuracy of the set-up and the required maximum size of the set-up. A two camera interferometer is more compact than a three camera interferometer. However, its measuring accuracy is lower. For this reason the new interferometer contains three cameras. A comprehensive description of both a two camera interferometer and a three camera interferometer can be found in chapter 2.

The measuring accuracy of the interferometer is not only dependent on the number of cameras in the set-up. For accurate measurements, the interference patterns on the CCD-cameras have to be mutually related. This requires a good mutual alignment of the cameras. The required alignment accuracy of the cameras is discussed in chapter 3. Finally, all other optical components in the set-up have to be adjusted optimally to realize an accurate interferometer. The required alignment accuracy of these components is described in chapter 4. Summarized conclusions regarding the measuring accuracy of the interferometer in relation to the alignment of all components can be found in chapter 5.

# 2. Two and three camera interferometers

## 2.1 Introduction

An interferometer measures the phase difference between its test beam and its reference beam. This phase difference can be caused by a refractive index profile in the test section of the interferometer, which is passed by the test beam and not by the reference beam. Under the assumption that the refractive index profile is two dimensional, i.e., it is constant in the propagation direction of the beam, the phase difference is linearly related to the refractive index. Because the refractive index is a spatially varying function, the phase difference is also a spatially varying function. The output intensity $I_0$ of a Michelson interferometer is given by:[1,2]

$$I_0 = I_t + I_r + 2\sqrt{I_t I_r}\cos\alpha \tag{2.1}$$

where $I_t$ is the intensity distribution in the test beam traversing the test section, $I_r$ is the intensity distribution in the reference beam, $\alpha$ is the phase difference between the test beam and the reference beam caused by the refractive index field in the test section. The phase $\alpha$ is the parameter of interest, $I_0$ is the measured intensity. Because of instabilities in the laser output, possible vibrations in the optical system and unsteadiness of the examined field, $I_t$, $I_r$ and $\alpha$ vary in time. So at an arbitrary time $t$ there are three unknowns in equation (2.1): $I_t+I_r$, $2\sqrt{I_t I_r}$ and $\alpha$. Two methods exist to solve equation (2.1) for the phase $\alpha$.

The first method is to measure $I_0$ simultaneously for three different externally applied phase shifts between the test beam and the reference beam. To achieve this goal a three camera detection system is required, measuring the intensities $I_{0,n}$ ($n$=0,1,2), respectively:

$$I_{0,n} = I_t + I_r + 2\sqrt{I_t I_r}\cos(\alpha + n\beta) \tag{2.2}$$

where ß is a known phase shift. Equation (2.2) defines a system of three equations with three unknowns from which $\alpha$ can be solved in the interval $[0,2\pi\rangle$.

The other method to solve the problem is to filter out the zero frequency component in the intensity distribution, i.e., $I_t+I_r$, by using a Fourier filter. By measuring the intensity distribution simultaneously for two different phase shifts, the system to be solved is:

$$I_{0,n} = 2\sqrt{I_t I_r}\ |\cos(\alpha + n\beta)| \tag{2.3}$$

where $n$=0,1. Equation (2.3) represents a system of two equations with two unknowns, from which $\alpha$ can be solved in the interval $[0,\pi\rangle$ if $\beta$ is not a multiple of $\pi/2$. In this case only a two camera detection system is required in the set-up.

In section 2.2 the two camera system is presented. Likewise the three camera system is presented in section 2.3. In section 2.4 a trade-off is made between both systems resulting in the choice to develop a three camera interferometer system.

## 2.2 A two camera interferometer

A Michelson interferometer system equipped with two cameras is shown in figure 2.1. The laser emits a beam which is polarised in the $x$-direction and which propagates along the $z$-axis. A half wave plate (hwp) with its fast axis under 22.5° with respect to the $x$-axis rotates the polarisation direction of the beam over 45°. The non-polarising beamsplitter (BS) splits the beam into two beams of equal intensities: a reflected beam, being the test beam, and a transmitted beam, being the reference beam. Both beams have a polarisation component in the $x$-direction as well as in the $y$-direction. The reference beam passes a quarter wave plate (qwp) with its fast axis at 45° to the $x$-axis. Now the beam consists of two circularly polarised components: one component is right circularly polarised, the other is left circularly polarised. In the ideal situation, i.e., beamsplitter BS splits the beam independently of the polarization state, the amplitudes of the circularly polarised components are equal, which implies that the polarisation state of the total beam is still linear. Next the beam passes a quarter wave plate rotating at the angular frequency $\omega'$ (rqwp), is reflected by the flat mirror M1 and passes the rotating quarter wave plate for the second time. Now the originally right circularly polarised component becomes left circularly polarised and frequency shifted over $2\omega'$. The originally left circularly polarised component becomes right circularly polarised and frequency shifted over $-2\omega'$. After having traversed the non-rotating quarter wave plate for the second time, the beam contains two perpendicularly plane polarised components. The $x$-polarised component is frequency shifted over $2\omega'$, the $y$-polarised component is frequency shifted over $-2\omega'$. After reflection by the beamsplitter, the test beam passes the test section, is reflected by

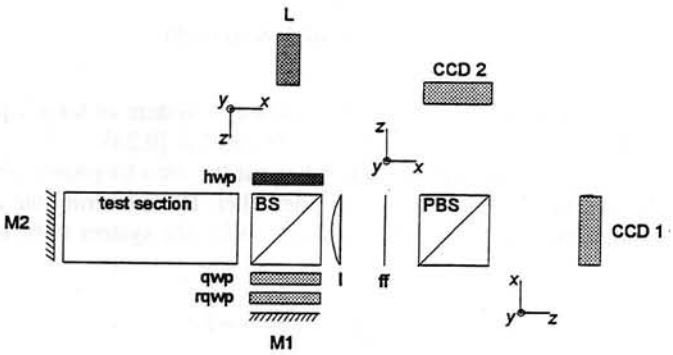


**Figure 2.1** A two camera interferometer. L=laser; BS=beamsplitter; PBS=polarising beamsplitter; hwp=half wave plate; qwp=quarter wave plate; rqwp=rotating qwp; M1,M2=plane mirror; l=lens; ff=Fourier filter.

the plane mirror M2 and passes the test section for the second time. As a consequence, the test beam is shifted in phase over $\alpha$.
The reference beam and test beam are recombined by the beamsplitter (BS). A lens images the beam on the CCD-cameras. The optical Fourier filter (ff) in the plane of focus filters out the DC-component in the intensity distribution. Next the beam is split by a polarising beamsplitter so that the *x*-polarised component is transmitted to CCD1 and the *y*-polarised component is reflected to CCD2. This implies that the intensity distribution on CCD1 results from the interaction between the test beam, which is phase shifted over $\alpha$, and the reference beam, which is frequency shifted over $2\omega'$. Similarly, on CCD2 there is interference between the test beam and the reference beam, which is frequency shifted over $-2\omega'$.

For a complete understanding of the interferometer, an analytical description is given below.
The laser beam's electric field vector $\boldsymbol{E}$ can be described by:

$$\boldsymbol{E} = \begin{bmatrix} A \\ 0 \end{bmatrix} e^{-i\omega t} \tag{2.4}$$

where $A$ is the amplitude of the electric field, $\omega$ is the angular frequency and $t$ the time. After having traversed the half wave plate, the electric field vector is given by:[3]

$$\boldsymbol{E} = -\frac{i}{\sqrt{2}} \begin{bmatrix} 1 & 1 \\ 1 & -1 \end{bmatrix} \begin{bmatrix} A \\ 0 \end{bmatrix} e^{-i\omega t} = -\frac{iA}{\sqrt{2}} \begin{bmatrix} 1 \\ 1 \end{bmatrix} e^{-i\omega t} \tag{2.5}$$

Just behind the beamsplitter the electric field of the reference beam $\boldsymbol{E}_r$ can be written as:

$$\boldsymbol{E}_r = -\frac{iA}{\sqrt{2}} \begin{bmatrix} c_{tx} \\ c_{ty} \end{bmatrix} e^{-i\omega t} \tag{2.6}$$

where $c_{tx}$ and $c_{ty}$ are the amplitude transmission coefficients of the beamsplitter for *x*- and *y*-polarised light, respectively: $c_{tx} \approx c_{ty} \approx 1/\sqrt{2}$. After having passed the fixed quarter wave plate, the electric field vector is:[3,4]

$$\boldsymbol{E}_r = -\frac{iA}{2} \begin{bmatrix} 1 & -i \\ -i & 1 \end{bmatrix} \begin{bmatrix} c_{tx} \\ c_{ty} \end{bmatrix} e^{-i\omega t} = -\frac{iA}{2} \begin{bmatrix} c_{tx} - ic_{ty} \\ -ic_{tx} + c_{ty} \end{bmatrix} e^{-i\omega t} \tag{2.7}$$

This is a summation of a right and left circularly polarised component. Next the beam

passes the rotating quarter wave plate, is reflected by the plane mirror M1 and passes the rotating quarter wave plate for the second time. This can be described as if the beam passes a half wave plate rotating with angular frequency $\omega'$. Now the electric field vector is:

$$\begin{aligned} \boldsymbol{E}_r &= -\frac{A}{2}\begin{bmatrix} cos2\omega' t & sin2\omega' t \\ sin2\omega' t & -\cos 2\omega' t \end{bmatrix}\begin{bmatrix} c_{tx} - ic_{ty} \\ -ic_{tx} + c_{ty} \end{bmatrix} e^{-i\omega t} \\ &= -\frac{Ac_{tx}}{2}\begin{bmatrix} 1 \\ i \end{bmatrix} e^{-i(\omega+2\omega')t} + \frac{Ac_{ty}}{2}\begin{bmatrix} i \\ 1 \end{bmatrix} e^{-i(\omega-2\omega')t} \end{aligned} \tag{2.8}$$

Having passed the fixed quarter wave plate, the electric field vector is:

$$\boldsymbol{E}_r = -\frac{Ac_{tx}}{\sqrt{2}}\begin{bmatrix} 1 \\ 0 \end{bmatrix} e^{-i(\omega+2\omega')t} + \frac{Ac_{ty}}{\sqrt{2}}\begin{bmatrix} 0 \\ 1 \end{bmatrix} e^{-i(\omega-2\omega')t} \tag{2.9}$$

The test beam traverses the test section twice, resulting in a phase shift of $\alpha$. With the use of equation (2.4) the electric field $\boldsymbol{E}_t$ can be written as:

$$\boldsymbol{E}_t = -\frac{iA}{\sqrt{2}}\begin{bmatrix} c_{rx} \\ c_{ry} \end{bmatrix} e^{-i(\omega t+\alpha)} \tag{2.10}$$

where $c_{rx}$ and $c_{ry}$ are the amplitude reflection coefficients of the beamsplitter for $x$- and $y$-polarised light, respectively: $c_{rx} \approx c_{ry} \approx 1/\sqrt{2}$.
The electric fields $\boldsymbol{E}_r$ and $\boldsymbol{E}_t$ are recombined by the beamsplitter. Now, the total electric field $\boldsymbol{E}_{tot}$ is the sum of $\boldsymbol{E}_r$ (equation (2.9)) and $\boldsymbol{E}_t$ (equation (2.10)) after they have been corrected for reflection by the beamsplitter and transmission through the beamsplitter, respectively. This correction implies multiplication of the x-component of equation (2.9) by $c_{rx}$, multiplication of the y-component of equation (2.9) by $c_{ry}$, multiplication of the x-component of equation (2.10) by $c_{tx}$ and multiplication of the y-component of equation (2.10) by $c_{ty}$. The total electric field $\boldsymbol{E}_{tot}$ can now be written as:

$$\boldsymbol{E}_{tot} = \begin{bmatrix} E_x \\ E_y \end{bmatrix} = \frac{A}{\sqrt{2}}\begin{bmatrix} c_x e^{-i(\alpha+\pi/2)} - c_x e^{-2i\omega' t} \\ c_y e^{-i(\alpha+\pi/2)} + c_y e^{2i\omega' t} \end{bmatrix} e^{-i\omega t} \tag{2.11}$$

where $c_x = c_{tx}c_{rx} \approx 1/2$ and $c_y = c_{ty}c_{ry} \approx 1/2$. The intensity distribution $I_x$ of the $x$-polarised light is:

$$I_x \propto E_x E_x^* = A^2 c_x^2 (1 + \sin(\alpha - 2\omega' t)) \tag{2.12}$$

Similarly, the intensity distribution $I_y$ of the $y$-polarised light is:

$$I_y \propto E_y E_y^* = A^2 c_y^2 (1 - \sin(\alpha + 2\omega' t)) \tag{2.13}$$

Since the DC-component in the intensity distribution is removed by the Fourier filter, the resulting intensity distributions are given by:

$$I_x \propto A^2 c_x^2 |\sin(\alpha - 2\omega' t)| \tag{2.14}$$

$$I_y \propto A^2 c_y^2 |\sin(\alpha + 2\omega' t)| \tag{2.15}$$

Because $x$-polarised light is transmitted by the polarising beamsplitter, equation (2.14) describes the intensity distribution on CCD1. Because $y$-polarised light is reflected by the polarising beamsplitter, the intensity distribution on CCD2 is given by equation (2.15).

Equations (2.14) and (2.15) define a system of two equations with three unknowns: $c_x^2$, $c_y^2$ and $\alpha$. The values of $c_x^2$ and $c_y^2$ are determined by the optical properties of the non-polarising beamsplitter. Although they depend on $x$ and $y$, they are system constants. The quotient $C = c_x^2 / c_y^2$ can be determined by dividing $I_x$ and $I_y$ when $\omega' = 0$. Equations (2.14) and (2.15) can be rewritten as:

$$I_x \propto A^2 C c_y^2 |\sin(\alpha - 2\omega' t)| \tag{2.16}$$

$$I_y \propto A^2 c_y^2 |\sin(\alpha + 2\omega' t)| \tag{2.17}$$

Under the assumption that $C$ and $\omega' t$ are exactly known, equations (2.16) and (2.17) describe a system of two equations with two unknowns ($A^2 c_y^2$ and $\alpha$). If $\omega' t$ is not a multiple of $\pi/2$, this system is solvable for $\alpha$ in the interval $[0,\pi\rangle$.

### 2.3 A three camera interferometer

In figure 2.2 a three camera Michelson interferometer set-up is shown. The light source is a red HeNe laser. The polarisation direction of the plane polarised beam, determined by a

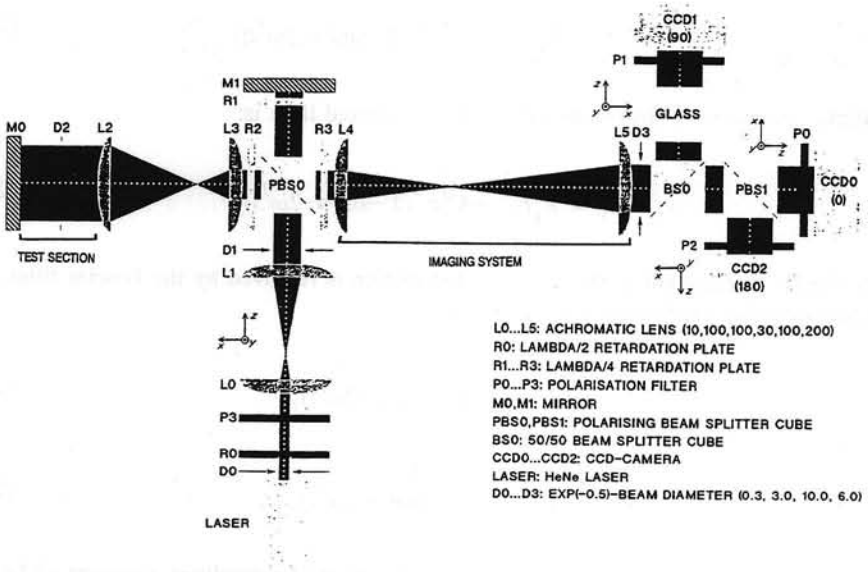


**Figure 2.2** A three camera Michelson interferometer.

half wave plate R0 in front of the laser, is at 45° to the *y*-axis (which is perpendicular to the plane of drawing). The remaining depolarised components are filtered out by polariser P3. The beam is expanded by the lens combination L0 and L1. Next the beam is split by the polarising beamsplitter PBS0. Because of the polarisation direction of the beam, the intensity of the transmitted reference beam and the intensity of the reflected test beam are almost equal. The test beam is expanded by the lens combination L2 and L3, traverses the test section twice and is shrinked to its original diameter again before it is transmitted by PBS0. It passes quarter wave plate R2 twice to obtain the right polarisation direction for transmission by PBS0. The reference beam is reflected by mirror M1. It passes quarter wave plate R1 twice to get the right polarisation direction for reflection by PBS0. Because the reference beam and the test beam are perpendicularly polarised after being recombined by PBS0, both beams are circularly polarised after having passed the quarter wave plate R3, whose fast axis is at 45° to the *y*-axis. The rotation directions of the two beams are opposite. Interference between the reference beam and the test beam occurs if all light is filtered out except the light polarised in one direction. The phase difference between the interfering beams is determined by the polarisation direction which is transmitted. After passage of the imaging system (lenses L4 and L5), the non-polarising beamsplitter BS and the polarising beamsplitter PBS1, light polarised in the *x*-direction reaches CCD0. The phase difference between the interfering beams is $\alpha-\pi/2$. Here $\alpha$ is the phase shift of the test beam relative to the reference beam due to the double passage through the test section. Similarly light at CCD2 is polarised in the *y*-direction. The phase difference between the interfering beams now is $\alpha+\pi/2$. If the non-polarising beamsplitter BS splits the beam independent of the polarisation state of the incoming beam and the transmitted polarisation direction of polariser P1 is at 45° to the *y*-axis, the interference pattern on

CCD1 is the result of interference between beams with a mutual phase shift $\alpha$. If beamsplitter BS does not split independently of the polarisation state, the same interference pattern results if the transmitted polarisation direction of polariser P1 is changed.

The imaging optics will be discussed in chapter 3. An analytical description of the set-up will be given in chapter 4, where an error analysis for the situation that the quarter wave plate R4 and polariser P2 are not perfectly adjusted.

## 2.4 Discussion

In section 2.2 a two camera interferometer was described, in section 2.3 a three camera interferometer. Here the advantages and disadvantages of the two camera interferometer relative to the three camera interferometer are discussed, so a clear choice can be made between the two systems.

The obvious advantage of the two camera interferometer when compared to the three camera interferometer is the use of a smaller number of cameras. This is advantageous because:

- Cameras are relatively expensive components.
- Each camera in the set-up has six degrees of freedom. All cameras in the set-up have to be mutually aligned with sub-pixel accuracy. This implies that the amount of degrees of freedom which have to be adjusted increases with a factor six for every extra camera. So a two camera interferometer has six degrees of freedom less to be aligned than a three camera interferometer. This implies that a two camera interferometer is easier to align.

The disadvantages of the two camera system are:

- Because of the use of equation (2.3) instead of equation (2.2), the interval in which $\alpha$ is measured by the two camera interferometer is $[0\text{-}\pi\rangle$, while it is $[0\text{-}2\pi\rangle$ for the three camera interferometer.
- $I_t$ and $I_r$ are not spatial constants as assumed in the analysis, but there are low frequency spatial variations in them due to the Gaussian intensity profile of the laser beam. A Fourier filter does not filter out the low frequency variations in the intensity distribution on the CCD-cameras due to the variations in $I_t$ and $I_r$ only, but also the low frequency variation in the intensity distribution due to low frequency variations in $\alpha$.
- The transmittance of a quarter wave plate will not be homogeneous over its surface. For this reason a rotating quarter wave plate will introduce undesired intensity fluctuations.
- To know the relative phase shift between the equations (2.16) and (2.17), $t$ has to be known exactly.

The disadvantages of the two camera system are directly related to the accuracy of the

whole measuring system. The advantages of the two camera system are related to the costs and the required effort to align the system. Because the accuracy of the system is most important, the three camera system is chosen for further development. Fortunately, as will be shown in chapter 3, the number of degrees of freedom per camera can be reduced from six to three if a suitable imaging system is used.

# 3. Alignment accuracies of the cameras

## 3.1 Introduction

In chapter 2 it has been shown that a Michelson interferometer equipped with three cameras is more accurate than one equipped with only two cameras. Therefore, from here on the attention will only be focused on the three camera set-up. The accuracy of this set-up is determined by the error in the measured phase shift between the test beam and the reference beam. This error depends on the alignment accuracies of the optical components and the accuracy of the normalization of the intensity levels on the CCD-cameras. The alignment accuracies of the cameras are analysed in this chapter. In chapter 4 the alignment accuracies of the quarter wave plate and the polariser will be analysed. Here also attention will be paid to the normalization of the intensity levels.

The phase shift $\alpha$ is a function of $x$ and $y$, i.e., the directions perpendicular to the propagation direction of the beam. If the relative phase shift between the beams is $\alpha(x,y)$ for CCD0, $\alpha(x,y)+\pi/2$ for CCD1 and $\alpha(x,y)+\pi$ for CCD2, $\alpha(x,y)$ can be calculated from the intensity distributions on the CCD-cameras:[1]

$$\alpha(x,y) = \arctan\left(\frac{I_2(x,y)-I_1(x,y)}{I_0(x,y)-I_1(x,y)}\right)+\frac{\pi}{4} \tag{3.1}$$

Here $I_0(x,y)$, $I_1(x,y)$ and $I_2(x,y)$ are the intensity distributions on CCD0, CCD1 and CCD2, respectively. As shown in figure 2.2 the direction of the $x$-axis is not the same for all cameras: the direction of the $x$-axis changes after reflection by beamsplitters BS and PBS1.

As shown in figure 3.1, each camera has six degrees of freedom: translation along the $x$-axis, the $y$-axis and the $z$-axis and rotation about the $x$-axis, the $y$-axis and the $z$-axis. Misalignment of any of these degrees of freedom of CCD$j$ ($j$=0,1,2) will lead to an error in $I_j(x,y)$ and hence to an error in the measured phase shift $\alpha(x,y)$, see equation (3.1). The subject of this chapter is to find out how accurate the cameras have to be aligned in all their degrees of freedom so that the error in $\alpha(x,y)$ will be smaller than 1% of $2\pi$. It will be shown in section 3.2 that the required alignment accuracy of the translation along the $x$-axis and the $y$-axis and the rotation about the $z$-axis are independent of the imaging optics used. The required alignment accuracy of the translation along the $z$-axis and the rotations about the $x$-axis and the $y$-axis, however,

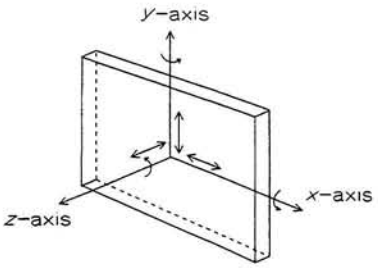


**Figure 3.1** The six degrees of freedom of a CCD-chip.

are dependent on the imaging optics. The required translational accuracy will be treated in section 3.3, the rotational accuracy in section 3.4.

### 3.2 Translation along the *x*-axis and the *y*-axis and rotation about the *z*-axis

In figure 3.2 the CCD-chips of CCD0, CCD1 and CCD2 are shown. Each chip is (partly) illuminated by an interference pattern, representing the interference between the test beam and the reference beam. It may not be expected in advance that the position of the beam is the same on all three CCD-chips. To describe this misalignment, in the surface of each chip a Cartesian coordinate system $(x,y)$ is defined. The origin is at the centre of the surface. Beside this coordinate system which is the same for each chip, a second Cartesian coordinate system $(x_0,y_0)$ is defined for CCD0. The $x_0$-axis and $y_0$-axis coincide with the surface of the chip and are parallel to the $x$-axis and the $y$-axis, respectively. The origin, however, is in the centre of the beam. Similarly, the Cartesian coordinate systems $(x_1,y_1)$ and $(x_2,y_2)$ are defined for CCD1 and CCD2, respectively. In the optical system (figure 2.2) the images on CCD0 and CCD2 are mirrored compared to the image on CCD1. However, mirroring of the coordinate systems is not shown in figure 3.2. Since the mirror operation is a standard image processing operation, this artefact of the set-up will not influence the present analysis.

The electric field $E_{t,j}$ on CCD$j$ due to the test beam can be described by:

$$E_{t,j}(x_j,y_j,t) = E_{0t}(x_j,y_j)\,e^{i(\omega t+\alpha+j\frac{\pi}{2})} \tag{3.2a}$$

where $E_{0t}$ is the (complex) amplitude of the electric field and $j$=0,1,2. Similarly, the electric field $E_{r,j}$ on CCD$j$ due to the reference beam is given by:

$$E_{r,j}(x_j,y_j,t) = E_{0r}(x_j,y_j)\,e^{i\omega t} \tag{3.2b}$$

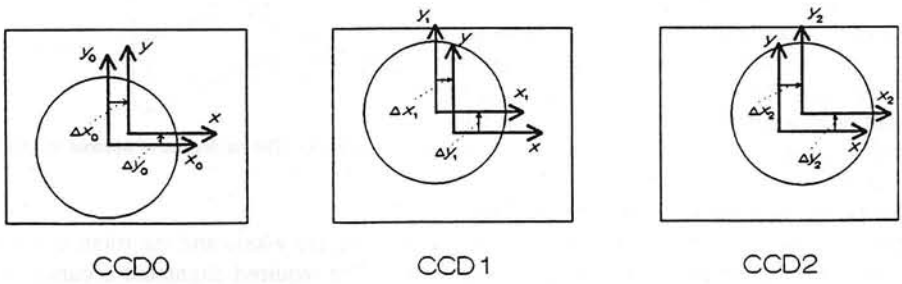


**Figure 3.2** Beam incident upon CCD-chips and the definitions of the coordinate systems.

Here $E_{0r}$ is the (complex) amplitude of the electric field of the reference beam. The intensity distribution in the interference pattern on CCD$j$ is proportional to the complex conjugate product of the sum electric field of the reference beam and the test beam:

$$I_j(x_j,y_j) \propto (E_{t,j}(x_j,y_j,t)+E_{r,j}(x_j,y_j,t))(E_{t,j}(x_j,y_j,t)+E_{r,j}(x_j,y_j,t))^*$$

$$\Rightarrow \tag{3.3a}$$

$$I_j(x_j,y_j) = I_{0t}(x_j,y_j)+I_{0r}(x_j,y_j)+2\sqrt{I_{0t}(x_j,y_j)I_{0r}(x_j,y_j)}\cos(\alpha+j\frac{\pi}{2})$$

Here $I_{0t}(x_j,y_j) \propto E_{0t}(x_j,y_j)E_{0t}^*(x_j,y_j)$ and $I_{0r}(x_j,y_j) \propto E_{0r}(x_j,y_j)E_{0r}^*(x_j,y_j)$ are the intensity distributions on CCD$j$ of the test beam and reference beam, respectively. These intensity distributions are assumed to be equal for $j$=0,1,2. Equation (3.3a) can be written as:

$$I_j(x_j,y_j) = I_B(x_j,y_j)+I_M(x_j,y_j)\cos(\alpha+j\frac{\pi}{2}) \tag{3.3b}$$

where $I_B$ is the bias intensity, which is defined as:

$$I_B(x_j,y_j) = I_{0t}(x_j,y_j)+I_{0r}(x_j,y_j) \tag{3.3c}$$

and $I_M$ is the modulation intensity, which is defined as:

$$I_M(x_j,y_j) = 2\sqrt{I_{0t}(x_j,y_j)I_{0r}(x_j,y_j)} \tag{3.3d}$$

By substituting equation (3.3b) and assuming $x_0=x_1=x_2=x$ and $y_0=y_1=y_2=y$, equation (3.1) can be obtained. This is the optimal situation: the centres of the beams coincide with the centres of the CCD-chips. In general $x_0 \neq x_1 \neq x_2 \neq x$ and $y_0 \neq y_1 \neq y_2 \neq y$ because of a misalignment of the CCD-chips along the $x$-axis and the $y$-axis. Then the measured phase $\alpha_M$ at the position $(x,y)$ becomes:

$$\alpha_M(x,y) = \arctan\left(\frac{I_2(x_2,y_2)-I_1(x_1,y_1)}{I_0(x_0,y_0)-I_1(x_1,y_1)}\right)+\frac{\pi}{4} \tag{3.4a}$$

If the coordinate system $(x_j,y_j)$ is shifted over $\Delta x_j$ the in $x$-direction and over $\Delta y_j$ in the $y$-direction compared to the coordinate system $(x,y)$, which implies $\Delta x_j=x_j-x$ and $\Delta y_j=y_j-y$, equation (3.4a) can be rewritten as:

$$\alpha_M(x,y,\Delta x_0,\Delta y_0,\Delta x_1,\Delta y_1,\Delta x_2,\Delta y_2) =$$

$$\arctan\left(\frac{I_2(x_2=x+\Delta x_2,y_2=y+\Delta y_2)-I_1(x_1=x+\Delta x_1,y_1=y+\Delta y_1)}{I_0(x_0=x+\Delta x_0,y_0=y+\Delta y_0)-I_1(x_1=x+\Delta x_1,y_1=y+\Delta y_1)}\right)+\frac{\pi}{4}= \qquad (3.4b)$$

$$\alpha(x,y)+\Delta\alpha(x,y,\Delta x_0,\Delta y_0,\Delta x_1,\Delta y_1,\Delta x_2,\Delta y_2)$$

where $\alpha(x,y)$ is the exact phase shift and $\Delta\alpha(x,y,\Delta x_0,\Delta y_0,\Delta x_1,\Delta y_1,\Delta x_2,\Delta y_2)$ is the error in the measured phase shift. By linearisation this error can be written as:

$$\Delta\alpha = \frac{d\alpha_M}{dx_0}\Delta x_0+\frac{d\alpha_M}{dy_0}\Delta y_0+\frac{d\alpha_M}{dx_1}\Delta x_1+\frac{d\alpha_M}{dy_1}\Delta y_1+\frac{d\alpha_M}{dx_2}\Delta x_2+\frac{d\alpha_M}{dy_2}\Delta y_2\Big|_{\substack{x_0=x_1=x_2=x\\ y_0=y_1=y_2=y}}^{x_0=x_1=x_2=x}$$

(3.4c)

where the dependence on $(x_j,y_j)$ has been omitted for notational simplicity. Substitution of equations (3.3b) and (3.4a) in equation (3.4c) gives:

$$\Delta\alpha(x,y,\Delta x_0,\Delta y_0,\Delta x_1,\Delta y_1,\Delta x_2,\Delta y_2) =$$

$$\frac{\cos\alpha-\sin\alpha}{2I_M}\left(\frac{dI_B}{dx}+\frac{dI_M}{dx}\cos\alpha-I_M\sin\alpha\frac{d\alpha}{dx}\right)\Delta x_0$$

$$+\frac{\cos\alpha-\sin\alpha}{2I_M}\left(\frac{dI_B}{dy}+\frac{dI_M}{dy}\cos\alpha-I_M\sin\alpha\frac{d\alpha}{dy}\right)\Delta y_0$$

$$-\frac{\cos\alpha}{I_M}\left(\frac{dI_B}{dx}-\frac{dI_M}{dx}\sin\alpha-I_M\cos\alpha\frac{d\alpha}{dx}\right)\Delta x_1$$

$$-\frac{\cos\alpha}{I_M}\left(\frac{dI_B}{dy}-\frac{dI_M}{dy}\sin\alpha-I_M\cos\alpha\frac{d\alpha}{dy}\right)\Delta y_1$$

$$+\frac{\cos\alpha+\sin\alpha}{2I_M}\left(\frac{dI_B}{dx}-\frac{dI_M}{dx}\cos\alpha+I_M\sin\alpha\frac{d\alpha}{dx}\right)\Delta x_2$$

$$+\frac{\cos\alpha+\sin\alpha}{2I_M}\left(\frac{dI_B}{dy}-\frac{dI_M}{dy}\cos\alpha+I_M\sin\alpha\frac{d\alpha}{dy}\right)\Delta y_2$$

where $\alpha$, $I_B$ and $I_M$ are functions of $x$ and $y$. Under the assumption that the intensity distributions in the test beam and the reference beam are equal, equations (3.3c) and (3.3d) yield:

$$I_B(x,y) = I_M(x,y) = 2I_{0t}(x,y) = 2I_{0r}(x,y) \tag{3.6}$$

If it is further assumed that $I_{0t}(x,y)$ and $I_{0r}(x,y)$ are Gaussian distributed, i.e.,

$$I_{0t}(x,y) = I_{0r}(x,y) = \frac{2P_0}{\pi w^2} e^{-2\frac{x^2+y^2}{w^2}} \tag{3.7a}$$

the first order derivatives of $I_{0t}(x,y)$ and $I_{0r}(x,y)$ with respect to $x$ and $y$ are given by:

$$\frac{dI_{0t}(x,y)}{dx} = \frac{dI_{0r}(x,y)}{dx} = -\frac{4x}{w^2} I_{0t}(x,y) = -\frac{4x}{w^2} I_{0r}(x,y) \tag{3.8a}$$

$$\frac{dI_{0t}(x,y)}{dy} = \frac{dI_{0r}(x,y)}{dy} = -\frac{4y}{w^2} I_{0t}(x,y) = -\frac{4y}{w^2} I_{0r}(x,y) \tag{3.8b}$$

Here $P_0$ is the total power in the individual beams and $w$ is the $e^{-2}$ waist at the CCD-surface. This waist is given by:

$$w = w_0 \sqrt{1 + \left(\frac{z\lambda}{\pi w_0^2}\right)^2} \tag{3.7b}$$

Here $\lambda$ is the wavelength of the light, $w_0$ the minimum $e^{-2}$-waist of the beam and $z$ the distance from the position where the waist is $w_0$. After substitution of equations (3.6), (3.8a) and (3.8b) in equation (3.5) it is easy to see that:

$$
\begin{aligned}
\Delta\alpha \;=\; & -2(\cos\alpha-\sin\alpha)(1+\cos\alpha)\frac{x\Delta x_0+y\Delta y_0}{w^2} \\
& -\frac{1}{2}(\cos\alpha-\sin\alpha)\sin\alpha\left(\frac{d\alpha}{dx}\Delta x_0+\frac{d\alpha}{dy}\Delta y_0\right) \\
& -4\cos\alpha(1-\sin\alpha)\frac{x\Delta x_1+y\Delta y_1}{w^2} \\
& +\cos^2\alpha\left(\frac{d\alpha}{dx}\Delta x_1+\frac{d\alpha}{dy}\Delta y_1\right) \\
& -2(\cos\alpha+\sin\alpha)(1-\cos\alpha)\frac{x\Delta x_2+y\Delta y_2}{w^2} \\
& +\frac{1}{2}(\cos\alpha+\sin\alpha)\sin\alpha\left(\frac{d\alpha}{dx}\Delta x_2+\frac{d\alpha}{dy}\Delta y_2\right)
\end{aligned}
\tag{3.9}
$$

From this equation an upper bound for the modulus of $\Delta\alpha$ can be deduced:

$$
\begin{aligned}
|\Delta\alpha| \;\le\; & 2\,|(\cos\alpha-\sin\alpha)(1+\cos\alpha)|\,\left|\frac{x\Delta x_0+y\Delta y_0}{w^2}\right| \\
& +\frac{1}{2}|(\cos\alpha-\sin\alpha)\sin\alpha|\,\left|\left(\frac{d\alpha}{dx}\Delta x_0+\frac{d\alpha}{dy}\Delta y_0\right)\right| \\
& +4\,|\cos\alpha(1-\sin\alpha)|\,\left|\frac{x\Delta x_1+y\Delta y_1}{w^2}\right| \\
& +\cos^2\alpha\,\left|\left(\frac{d\alpha}{dx}\Delta x_1+\frac{d\alpha}{dy}\Delta y_1\right)\right| \\
& +2\,|(\cos\alpha+\sin\alpha)(1-\cos\alpha)|\,\left|\frac{x\Delta x_2+y\Delta y_2}{w^2}\right| \\
& +\frac{1}{2}\,|(\cos\alpha+\sin\alpha)\sin\alpha|\,\left|\left(\frac{d\alpha}{dx}\Delta x_2+\frac{d\alpha}{dy}\Delta y_2\right)\right|
\end{aligned}
\tag{3.10}
$$

Averaging over $\alpha$ while assuming that the first order derivatives of $\alpha$ are independent of $\alpha$ gives:

$$|\Delta\alpha|_{ave} \leq \frac{5.66}{2\pi}\left|\frac{2(x\Delta x_0+y\Delta y_0)}{w^2}\right| + \frac{3.57}{4\pi}\left|\left(\frac{d\alpha}{dx}\Delta x_0+\frac{d\alpha}{dy}\Delta y_0\right)\right|$$
$$+\frac{8.00}{2\pi}\left|\frac{2(x\Delta x_1+y\Delta y_1)}{w^2}\right| + \frac{1}{2}\left|\left(\frac{d\alpha}{dx}\Delta x_1+\frac{d\alpha}{dy}\Delta y_1\right)\right| \qquad (3.11)$$
$$+\frac{5.66}{2\pi}\left|\frac{2(x\Delta x_2+y\Delta y_2)}{w^2}\right| + \frac{3.57}{4\pi}\left|\left(\frac{d\alpha}{dx}\Delta x_2+\frac{d\alpha}{dy}\Delta y_2\right)\right|$$

where $|\Delta\alpha|_{ave}$ is the average modulus of $\Delta\alpha$. Equation (3.11) shows that the influence of $\Delta x_0$, $\Delta x_2$, $\Delta y_0$ and $\Delta y_2$ on $|\Delta\alpha|_{ave}$ are equal. The influence of $\Delta x_1$ and $\Delta y_1$ is larger, because the multiplicative constants of the terms containing $\Delta x_1$ and $\Delta y_1$ are larger than the multiplicative constants of the terms containing $\Delta x_0$, $\Delta y_0$ and $\Delta x_2$, $\Delta y_2$. This implies that if CCD1 is chosen to be the reference camera, i.e., $\Delta x_1=\Delta y_1=0$, $|\Delta\alpha|_{ave}$ is minimised. Under the assumptions $\Delta x_0=\Delta y_0=\Delta x_2=\Delta y_2=\Delta x$ and $d\alpha/dx=d\alpha/dy$, this minimum value of $|\Delta\alpha|_{ave}$ can be written as:

$$|\Delta\alpha|_{ave} \leq \frac{22.64}{2\pi}\left|\frac{(x+y)\Delta x}{w^2}\right| + \frac{7.14}{2\pi}\left|\frac{d\alpha}{dx}\Delta x\right| \qquad (3.12a)$$

In the case that the assumptions are not valid and some of the parameters $\Delta x_0$, $\Delta y_0$, $\Delta x_2$ and $\Delta y_2$ are smaller than $\Delta x$ or $d\alpha/dy<d\alpha/dx$, then $|\Delta\alpha|_{ave}$ will be smaller than the value given by equation (3.12a). This equation can now be seen as an upper bound of $|\Delta\alpha|_{ave}$. For $w\rightarrow\infty$ inequality (3.12a) transforms into:

$$|\Delta\alpha|_{ave} \leq \frac{7.14}{2\pi}\left|\frac{d\alpha}{dx}\right||\Delta x| \qquad (3.12b)$$

If $|\Delta\alpha|_{ave}$ is required to be smaller than 1% of $2\pi$ the next upper bound for $|d\alpha/dx|$ is found:

$$\left|\frac{d\alpha}{dx}\right| \leq \frac{0.12\pi}{7.14\,|\Delta x|} \qquad (3.12c)$$

In the case of 2/3" CCD-chips, the pixels are about 10$\mu$m square and the total sensitive surface is about 6×4mm. This implies that the chips contain about 600×400 pixels. If the alignment accuracy of the chip is half a pixel for both translation along the $x$-axis and translation along the $y$-axis (i.e., 5 $\mu$m), equation (3.12c) requires $|d\alpha/dx|$ to be smaller than $10^4 m^{-1}$ to keep $|\Delta\alpha|_{ave}$ smaller than 1% of $2\pi$. This implies that at least 59 pixels are needed per fringe, so that the maximum number of fringes on the CCD-chip is about

10 in the horizontal direction and 7 in the vertical direction. However, it is desirable to analyse fringe patterns whose fringe densities are a factor 10 higher. This implies that a gradient of at least $|d\alpha/dx| = 10^5 m^{-1}$ has to be measurable. To keep $|\Delta\alpha|_{ave}$ smaller than 1% of $2\pi$, equation (3.12c) now requires a translational accuracy of at least $\Delta x = 0.5\mu m$. This implies at least 6 pixels per fringe.

Now the translational accuracy along the $x$-axis and the $y$-axis are known ($0.5\mu m$), it is easy to calculate from them the required accuracy for rotation about the $z$-axis. The rotation and the translation are coupled to each other, see figure 3.3. When the rotation about the $z$-axis $\rho_z$ is small, it can locally be seen as a translation $\Delta y$ at a distance $r$ from the axis:

$$r\rho_z \approx \Delta y \qquad (3.13)$$

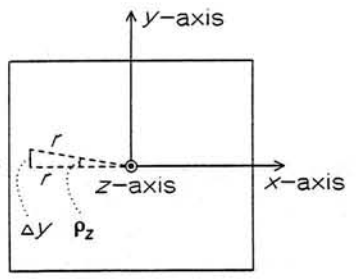


**Figure 3.3** A small rotation $\rho_z$ of a CCD-chip about the z-axis.

see figure 3.3. Given a maximum value of the translation $\Delta y$, the allowed maximum value of $\rho_z$ depends on the maximum value for $r$. If the $z$-axis is in the centre of a 6mm CCD-chip, the maximum value of $r$ is 3mm. This means that if a translation of $0.5\mu m$ corresponds to an error of 1% of $2\pi$ in $\alpha$, then a rotation of $0.01^0$ will yield the same error. As will be clear, the error is maximum at the edges of the CCD-chip and will be smaller for $r<3mm$.

In the above derivation several assumptions were made. The question which remains to be answered is how these assumptions affect the maximum value of $|d\alpha/dx|$.

- The assumption $w \to \infty$ implies that the true value of $|d\alpha/dx|$ will be smaller than calculated. However, the modulus signs in equation (3.10) imply that an upper bound on $\Delta x$ is calculated, corresponding with a lower bound on $|d\alpha/dx|$. So the two approximations have an opposite effect on the maximum value of $|d\alpha/dx|$.
- For a one dimensional fringe pattern (i.e., a fringe pattern whose intensity distribution only varies in one direction), the maximum value of $|d\alpha/dx|$ is larger than calculated here. For $w \to \infty$ the value increases by a factor 2.
- In general the maximum value of $d\alpha/dx$ increases with the allowed error in $\alpha$. According to equation (3.12b), a linear relation exists.

In summary, to analyse fringe patterns with a fringe density of 1 fringe per 6 pixels, a translational accuracy of $0.5\mu m$ and a rotational accuracy of $0.01^0$ are required. Under the assumption that the accuracy of the translation along the $z$-axis and the rotation about the $x$-axis and $y$-axis are infinite, the average error in $\alpha$ will be about 2% of $2\pi$: about 1% due to the limited translational accuracy along the $x$-axis and the $y$-axis and about 1% due to the limited rotational accuracy about the $z$-axis. There exists an almost linear relation between the translational and the rotational accuracy and the average error in $\alpha$. For $w \to \infty$ an almost linear relation exists between $d\alpha/dx$ and the average error in $\alpha$, which implies an almost linear relation between the average error and the fringe density on the CCD-

chip.

### 3.3 Translation along the $z$-axis

In figure 2.2 the experimental set-up is shown. A laser beam with an $e^{-1/2}$-beam diameter of 0.3mm is expanded to a beam with an $e^{-1/2}$- beam diameter of 3.0mm. After reflection by PBS0 the test beam diameter is expanded to 10.0 mm before entering the test section. The whole system of lenses L2, L3 and an imaging system images a plane in the test section on the CCD-chips. The $e^{-1/2}$-diameter of the illuminated part of the plane is 10.0mm. To image it on a 6mm diameter CCD-chip, a lateral magnification factor of 3/5 is required for the lens combination L2, L3 and the imaging system. Because this magnification factor of the lens combination L2, L3 is 3/10, a lateral magnification factor of 2 is required for the imaging system. The imaging system may consist of two lenses or a single lens. The imaging system determines the translational accuracy of the CCD-chips along the $z$-axis. In this section this translational accuracy is calculated for both imaging systems. The results show that a two lens imaging system is preferred.

In figure 3.4 imaging in the interferometer by the single lens imaging system is shown. The focal length of the single lens imaging system, i.e., lens L4, is 80 mm. This relatively large focal length is needed to obtain an imaging distance, which is large enough to position optical components like beamsplitters and polarisers between the lens and the CCD-cameras. The object plane of lens L4 is the image plane of lens combination L2, L3. This plane is at a distance of $3f_4/2$ in front of lens L4 to obtain a magnification of 2 in the image plane at a distance of $3f_4$ behind the lens. If the disturbances in the test beam by the medium in the test section are small, the beam is almost paraxial Gaussian. The

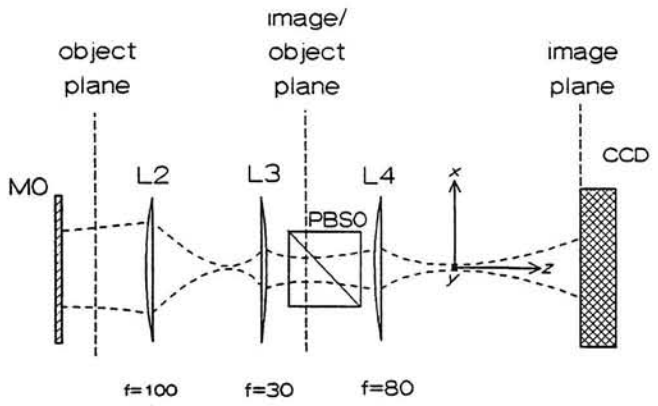


**Figure 3.4** Imaging in the interferometer by a single lens imaging system.
The symbols are from figure 2.2.

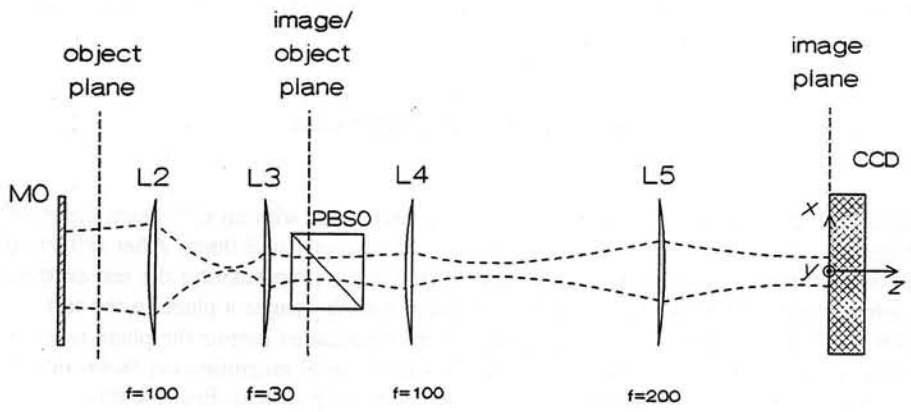


**Figure 3.5** Imaging in the interferometer by a two lens imaging system. The symbols are from figure 2.2.

minimal beam waist of the beam behind L4 is in the focal plane of the lens. After this minimal waist the beam is expanding. This means that the beam is expanding in the image plane. Because of this expansion the magnification factor of the image depends strongly on the exact position of the imaging plane, i.e., the position of the CCD-chip along the *z*-axis.

In figure 3.5 imaging by a two lens imaging system (lenses L4 and L5) is shown. The focal planes of L4 and L5 coincide. To realize a magnification factor of 2 and a sufficient image distance, the focal lengths $f_4$=100 mm and $f_5$=200 mm were chosen for the lenses L4 and L5, respectively. If the object plane is the focal plane of L4, then the image plane is in the focal plane of L5. If the beam is paraxial, then the minimal waist behind the imaging system is also in the focal plane of L5. This implies that the position of the image plane and the position of minimum beam waist coincide. Now the first order derivative of the beam waist is zero in the image plane and so the magnification of the beam is almost constant in some interval along the *z*-axis. This implies that the positioning of the CCD-chip is not critical: it can be positioned anywhere in this interval. So a two lens imaging system requires a lower translational accuracy of the CCD-cameras along the *z*-axis than a single lens imaging system.

The fact that the single lens imaging system requires a better translational accuracy for the CCD-chip than a two lens imaging system can be further clarified by looking at the set-up in a different way. In this alternative approach the whole lens system for imaging a plane in the test section is considered, i.e., the combination of L2, L3 and the imaging system in figures 3.4 and 3.5. When the single lens imaging system is used, a small translation of the CCD-chip along the *z*-axis leads to a change of both the position of the object plane in the test section and the magnification of the image in relation to the object. When the two lens imaging system is used, however, a small translation of the CCD-chip around its optimal position only leads to a displacement of the object plane. The magnification of the

image remains the same. So it is easy to see that the position of the CCD-chip is more critical for a single lens system than for a two lens system.

To calculate the required alignment accuracy of the CCD-cameras, a relation has to be known between the misalignment of the CCD-chip and the error in the measured phase due to this misalignment. Below this relation will be derived for both the single lens imaging system and the two lens imaging system. The required translational accuracy is calculated for the situation that $|\Delta\alpha|_{ave}$ has to be smaller than 1% of $2\pi$.

For both the single lens imaging system and the two lens imaging system, a Cartesian coordinate system $(x,y,z)$ is defined in the beam behind the imaging system, see figures 3.4 and 3.5. The $z$-axis is defined on the optical axis of the beam, the position of the origin is the position of minimal waist. With equations (3.3b) and (3.6) the intensity distribution $I_j(x,y,G)$ on CCD$j$ can be written as:

$$I_j(x,y,G) = \frac{1}{G^2} I_j\left(\frac{x}{G},\frac{y}{G}\right) = \frac{2}{G^2} I_{0,t}\left(\frac{x}{G},\frac{y}{G}\right)\left(1+\cos\left(\alpha\left(\frac{x}{G},\frac{y}{G}\right)+j\frac{\pi}{2}\right)\right) \tag{3.14a}$$

where $G$ is the magnification factor of the beam waist compared to the minimal waist and $j$=0,1,2. If $I_{0t}$ (and $I_{0r}$) has a Gaussian intensity distribution equation (3.14a) can be written as:

$$I_j(x,y,G) = \frac{4P_0}{\pi G^2 w_0^2}\, e^{-2\frac{x^2+y^2}{G^2 w_0^2}} \left(1+\cos\left(\alpha\left(\frac{x}{G},\frac{y}{G}\right)+j\frac{\pi}{2}\right)\right) \tag{3.14b}$$

Here $P_0$ is the power of the test/reference beam, $w_0$ is the minimal beam waist and $G$ is a function of $z$ given by:

$$G = \frac{w}{w_0} = \sqrt{1+\left(\frac{z\lambda}{\pi w_0^2}\right)^2} \tag{3.15}$$

If the CCD-chips are perfectly aligned for translation along the $x$-axis and the $y$-axis and for all rotations, then the measured phase $\alpha_M$ can be written as:

$$\alpha_M(x,y,G_0,G_1,G_2) = \arctan\left(\frac{I_2(x,y,G_2)-I_1(x,y,G_1)}{I_0(x,y,G_0)-I_1(x,y,G_1)}\right)+\frac{\pi}{4} \tag{3.16a}$$

where $G_j$ is the magnification factor of the beam waist on CCD$j$. This can be written as:

$$\alpha_M(x,y,G_0,G_1,G_2) = \alpha(x,y,G_0=G_e,G_1=G_e,G_2=G_e) + \Delta\alpha(x,y,\Delta G_0,\Delta G_1,\Delta G_2) \tag{3.16b}$$

Here $G_e$ is the magnification factor of the beam waist at the CCD-chip if the chip would be positioned perfectly in the image plane at $z=z_e$. Then the measured phase is $\alpha(x,y,G_0=G_e,G_1=G_e,G_2=G_e)$. Due to misalignment of CCD$j$, the position $z_j$ of the CCD-chip is unequal to $z_e$ and the magnification of the beam waist on the CCD-chip $G_j$ differs a factor $\Delta G_j$ from $G_e$: $\Delta G_j=G_j-G_e$. The error in the measured phase due to the misalignment is given by $\Delta\alpha(x,y,\Delta G_0,\Delta G_1,\Delta G_2)$. Here the phase error is not written as a function of the misalignment of the CCD-chips, but as a function of the magnification errors $\Delta G_j$ of the beam waists due to the misalignment of the chips. Linearisation of $\alpha$ with respect to $G_0$, $G_1$ and $G_2$ gives for $\Delta\alpha(x,y,\Delta G_0,\Delta G_1,\Delta G_2)$:

$$\Delta\alpha(x,y,\Delta G_0,\Delta G_1,\Delta G_2) = \frac{d\alpha}{dG_0}\Delta G_0 + \frac{d\alpha}{dG_1}\Delta G_1 + \frac{d\alpha}{dG_2}\Delta G_2 \Big|_{G_0=G_1=G_2=G_e} \tag{3.16c}$$

Substituting equation (3.16a) and using equation (3.14b) gives:

$$\begin{aligned}
&\Delta\alpha(x,y,\Delta G_0,\Delta G_1,\Delta G_2) = \\
&\frac{1}{2}(\cos\alpha-\sin\alpha)\left\{\left(-\frac{2}{G_e}+4\frac{x^2+y^2}{G_e^3 w_0^2}\right)(1+\cos\alpha)+\sin\alpha\left(\frac{d\alpha}{d(\frac{x}{G_e})}\frac{x}{G_e^2}+\frac{d\alpha}{d(\frac{y}{G_e})}\frac{y}{G_e^2}\right)\right\}\Delta G_0 \\
&+\cos\alpha\left\{\left(-\frac{2}{G_e}+4\frac{(x^2+y^2)}{G_e^3 w_0^2}\right)(1-\sin\alpha)+\cos\alpha\left(\frac{d\alpha}{d(\frac{x}{G_e})}\frac{x}{G_e^2}+\frac{d\alpha}{d(\frac{y}{G_e})}\frac{y}{G_e^2}\right)\right\}\Delta G_1 + \\
&+\frac{1}{2}(\cos\alpha+\sin\alpha)\left\{\left(-\frac{2}{G_e}+4\frac{x^2+y^2}{G_e^3 w_0^2}\right)(1-\cos\alpha)-\sin\alpha\left(\frac{d\alpha}{d(\frac{x}{G_e})}\frac{x}{G_e^2}+\frac{d\alpha}{d(\frac{y}{G_e})}\frac{y}{G_e^2}\right)\right\}\Delta G_2
\end{aligned} \tag{3.16d}$$

where $\alpha$ is a function of $x/G_e$ and $y/G_e$. From this expression an upper bound for the modulus of the phase error can be found:

$$
\begin{aligned}
|\Delta\alpha| \le & \left| -\frac{1}{G_e} + 2\frac{x^2+y^2}{G_e^3 w_0^2} \right| |(\cos\alpha - \sin\alpha)(1+\cos\alpha)| \; |\Delta G_0| \\
& + \left| \frac{d\alpha}{d(\frac{x}{G_e})} \frac{x}{2G_e^2} + \frac{d\alpha}{d(\frac{y}{G_e})} \frac{y}{2G_e^2} \right| |(\cos\alpha - \sin\alpha)\sin\alpha| \; |\Delta G_0| \\
& + 2\left| -\frac{1}{G_e} + 2\frac{x^2+y^2}{G_e^3 w_0^2} \right| |\cos\alpha(1-\sin\alpha)| \; |\Delta G_1| \\
& + 2\left| \frac{d\alpha}{d(\frac{x}{G_e})} \frac{x}{2G_e^2} + \frac{d\alpha}{d(\frac{y}{G_e})} \frac{y}{2G_e^2} \right| \cos^2\alpha \; |\Delta G_1| \\
& + \left| -\frac{1}{G_e} + 2\frac{x^2+y^2}{G_e^3 w_0^2} \right| |(\cos\alpha + \sin\alpha)(1-\cos\alpha)| \; |\Delta G_2| \\
& + \left| \frac{d\alpha}{d(\frac{x}{G_e})} \frac{x}{2G_e^2} + \frac{d\alpha}{d(\frac{y}{G_e})} \frac{y}{2G_e^2} \right| |(\cos\alpha + \sin\alpha)\sin\alpha| \; |\Delta G_2|
\end{aligned}
\tag{3.16e}
$$

Averaging over $\alpha$ and assuming $\Delta G_0 = \Delta G_1 = \Delta G_2 = \Delta G$ gives:

$$
|\Delta\alpha|_{ave} \le \left\{ 3.07 \left| -\frac{1}{G_e} + 2\frac{x^2+y^2}{G_e^3 w_0^2} \right| + 1.07 \left| \frac{d\alpha}{dx}\frac{x}{G_e} + \frac{d\alpha}{dy}\frac{y}{G_e} \right| \right\} |\Delta G| \tag{3.16f}
$$

In the case that $\Delta G_0$, $\Delta G_1$ or $\Delta G_2$ is smaller than $\Delta G$, then $|\Delta\alpha|_{ave}$ is smaller than the value given by this equation. This value can now be seen as an upper bound.
In equation (3.16f) $|\Delta\alpha|_{ave}$ is dependent on $x$ and $y$. To obtain an upper bound for $|\Delta\alpha|_{ave}$ which is independent of these parameters, the two terms on the right-hand side have to be maximised. The first term is maximised by choosing $x=y=0$. Under the assumption that $d\alpha/dx = d\alpha/dy$ and that the CCD-chips have a diameter of $G_e w_0$, the second term is maximised by choosing $x=y=G_e w_0/2$. In this case $|\Delta\alpha|_{ave}$ can be estimated by:

$$|\Delta\alpha|_{ave} < \left\{ \frac{3.07}{|G_e|} + 1.07 w_0 \left| \frac{d\alpha}{dx} \right| \right\} |\Delta G| \qquad (3.16g)$$

To find $|\Delta\alpha|_{ave}$ as a function of the misalignment $\Delta z$ of the CCD-chip, the relation between $\Delta G$ and $\Delta z$ has to be known. For a single lens imaging system this relation can be found by linearisation of equation (3.15) with respect to $z$ about $z_e$:

$$|\Delta G| = \left| \frac{dG}{dz}\Big|_{z=z_e} \Delta z \right| = \frac{|z_e|}{G_e} \left( \frac{\lambda}{\pi w_0^2} \right)^2 |\Delta z| \qquad (3.17)$$

where $\lambda$ is the wavelength of the light. Substitution in equation (3.16g) gives:

$$|\Delta z| < \frac{|\Delta\alpha|_{ave}}{\frac{3.07}{G_e} + 1.07 w_0 \left| \frac{d\alpha}{dx} \right|} \frac{G_e}{|z_e|} \left( \frac{\pi\omega_0^2}{\lambda} \right)^2 \qquad (3.18a)$$

Here $|\Delta\alpha|_{ave}$ is the maximum average modulus of the error in $\alpha$ found to be acceptable by the user. In the set-up of figure 3.4 a lens L4 with a focal length $f_4$=80mm is used. To realize a magnification factor of 2, $z_e$ must be equal to 160mm. The minimum waist $w_0$ behind lens L4 is 5.4 $\mu$m, as can easily be verified by using the theory of Gaussian optics. Under the assumptions that a 632.8nm laser is used, that the maximum phase gradient $|d\alpha/dx|$ is $10^5 m^{-1}$ (six pixels per fringe, see section 3.2) and that the average modulus of the error in $\alpha$ is 1% of $2\pi$, then equation (3.18a) requires $|\Delta z|$ to be smaller than 15$\mu$m. The second term in the denominator of equation (3.18a) dominates the first term, so the error is determined by the change in the intensity distribution in the fringes.

To estimate $\Delta z$ for the two lens imaging system, equation (3.17) cannot be used. Because the image is in the focus (i.e., $z_e$=0), $dG/dz$ is zero at $z=z_e=0$ and the first order approximation of $|\Delta G|$ (equation (3.17)) is also zero. To find a second order relation between $|\Delta G|$ and $|\Delta z|$, $G$ (equation (3.15)) is expanded with respect to $z$ and $G_e$=1 is subtracted:

$$|\Delta G| = \frac{1}{2} \left( \frac{\Delta z \, \lambda}{\pi w_0^2} \right)^2 \qquad (3.19)$$

Here $\Delta z=z$ because $z_e$=0. Substitution of equation (3.19) in equation (3.16g) gives:

$$|\Delta z| < \frac{\pi w_0^2}{\lambda}\sqrt{\frac{2\,|\Delta\alpha|_{ave}}{\frac{3.07}{G_e}+1.07 w_0\left|\frac{d\alpha}{dx}\right|}} \qquad (3.18b)$$

where $G_e$=1 because the image is at the position of the minimal waist. When equation (3.18b) is applied to the set-up of figure 2.2 ($\lambda$=632.8 nm, $f_4$=100m, $f_5$=200mm and $w_0$=6 mm) under the assumption $d\alpha/dx=d\alpha/dy<10^5 m^{-1}$, an upper bound for $|\Delta z|$ of 2.4 m results if $|\Delta\alpha|_{ave}$ is required to be smaller than 1% of $2\pi$. Again the change in intensity distribution due to the fringes dominates the change in intensity distribution due to the changing profiles of the reference and test beam.

When the translational accuracies found above are compared, it can be concluded that the single lens imaging system requires a much better translational accuracy than the two lens imaging system. When $|d\alpha/dx|<10^5 m^{-1}$ and $|\Delta\alpha|_{ave}$ is smaller than 1% of $2\pi$, the required translational accuracy for the CCD-chip along the $z$-axis is $|\Delta z|=15\mu m$ for the single lens system. For the two lens system, however, this accuracy is 2.4 m. This implies that for a single lens imaging system the translation of the CCD-chip along the $z$-axis is a serious degree of freedom, which has to be adjusted exactly. For the two lens imaging system, however, this translation is not a serious degree of freedom. So an interferometer equipped with a two lens imaging system is much easier to align than an interferometer equipped with a single lens imaging system.

### 3.4 Rotation about the $x$-axis and the $y$-axis

The CCD's last degree of freedom due to which errors in the measured value of $\alpha$ can occur is a rotation of the CCD-chip about any axis through O in the $xy$-plane. In this section $|\Delta\alpha|_{ave}$ due to a rotation of the CCD-chip about the $y$-axis will be calculated. The result, however, is valid for rotation about any axis in the $xy$-plane through O.

In figure 3.6 the parallel beam leaving the two lens imaging system is incident upon the chip of CCD$j$. A Cartesian coordinate system $(x,y)$ is defined perpendicular to the propagation direction of the beam. Its origin is in the centre of the beam and on the CCD-surface. The CCD-chip is rotated

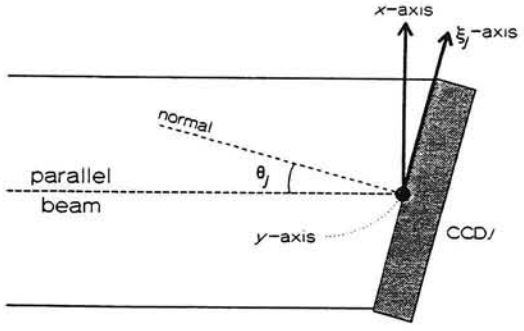


**Figure 3.6** A parallel beam is incident on the chip of CCDj, which is rotated $\theta_j$ around the y-axis.

about the $y$-axis, so there is an angle $\theta_j$ between the propagation direction of the beam and the normal on the CCD-surface. Parallel to the CCD-surface and perpendicular to the $y$-axis, an $\xi_j$-axis is defined. Its origin coincides with the origin of the coordinate system $(x,y)$, so there is an angle $\theta_j$ between the $x$-axis and $\xi_j$-axis. The intensity distribution in the beam is the result of interference between the interferometer's reference beam and test beam. Because the beam is assumed to be parallel, the interferometer's reference beam and test beam are parallel too, i.e., $w=w_0$. Under the assumption that the test beam and the reference beam have a Gaussian intensity distribution, the intensity distribution $I_j$ in the beam illuminating CCD$j$ can be calculated by substituting equations (3.6) and (3.7) in equation (3.3b):

$$I_j(x,y) = \frac{4P_0}{\pi w_0^2} e^{-2\frac{x^2+y^2}{w_0^2}} \left(1+\cos\left[\alpha(x,y)+j\frac{\pi}{2}\right]\right) \tag{3.19}$$

The intensity distribution $I_{j,M}$ measured by CCD$j$ differs from this intensity distribution for two reasons:

- the beam waist in $\xi_j$-direction is a factor $1/\cos\theta_j$ larger than in $x$-direction, so the effective beam surface is larger while the same power is passing through,
- the fringe pattern is scaled by a factor $1/\cos\theta_j$ compared to the $x$-direction.

Therefore the intensity distribution on CCD$j$ can be described as:

$$I_{j,M}(\xi_j,y) = \frac{4P_0\cos\theta_j}{\pi w_0^2} e^{-2\frac{\xi_j^2\cos^2\theta_j+y^2}{w_0^2}} \left(1+\cos\left[\alpha(\xi_j\cos\theta_j,y)+j\frac{\pi}{2}\right]\right) \tag{3.20}$$

where the coordinate $\xi_j$ is given by:

$$\xi_j = \frac{x}{\cos\theta_j} \tag{3.21}$$

So the phase shift $\alpha_M(\xi,y)$ measured with a three camera interferometer is:

$$\alpha_M(\xi_0,\xi_1,\xi_2,y) = \arctan\left(\frac{I_{2,M}(\xi_2,y)-I_{1,M}(\xi_1,y)}{I_{0,M}(\xi_0,y)-I_{1,M}(\xi_1,y)}\right) + \frac{\pi}{4} \tag{3.22a}$$

which will be interpreted as:

$$\alpha(x,y) = \arctan\left(\frac{I_2(x,y)-I_1(x,y)}{I_0(x,y)-I_1(x,y)}\right) + \frac{\pi}{4} \qquad (3.22b)$$

To approximate the error $\Delta\alpha$ in the phase shift made by the interferometer due to a small rotation about the $y$-axis, equation (3.22a) should be expanded linearly to $\theta_0$, $\theta_1$ and $\theta_2$ about $\theta_0=\theta_1=\theta_2=0$ (i.e., $\xi_0=\xi_1=\xi_2=x$). However, $I_{j,M}$ is only dependent on $\theta_j$ by cosine terms, so the first order derivative of $I_{j,M}$ with respect to $\theta_j$ is zero for $\theta_j=0$. This implies that the first order derivatives of $\alpha_M$ with respect to $\theta_0$, $\theta_1$ and $\theta_2$ are zero for $\theta_0=\theta_1=\theta_2=0$ ($\xi_j=x$) and a second order approximation of the error has to be made. This second order approximation can be obtained by expansion of equation (3.22a) to $\cos\theta_0$, $\cos\theta_1$ and $\cos\theta_2$ about $\cos\theta_0=\cos\theta_1=\cos\theta_2=1$ (that is $\xi_j=x$):

$$\begin{aligned}\Delta\alpha(\xi_0,\xi_1,\xi_2,y) = {} & \frac{d\alpha_M}{dI_{0,M}}\frac{dI_{0,M}}{d(\cos\theta_0)}\Big|_{\cos\theta_j=1}\Delta\cos\theta_0 \\ & + \frac{d\alpha_M}{dI_{1,M}}\frac{dI_{1,M}}{d(\cos\theta_1)}\Big|_{\cos\theta_j=1}\Delta\cos\theta_1 \qquad (3.23a) \\ & + \frac{d\alpha_M}{dI_{2,M}}\frac{dI_{2,M}}{d(\cos\theta_2)}\Big|_{\cos\theta_j=1}\Delta\cos\theta_2 \qquad (j=0,1,2)\end{aligned}$$

where $\Delta\cos\theta_j=\cos\theta_j-1$. Here equations (3.20) and (3.22a) can be substituted. The fact that the first order derivative of $\alpha_M$ with respect to $I_{j,M}$ and the first order derivative of $I_{j,M}$ with respect to $\cos\theta_j$ are evaluated at $\cos\theta_j=1$ ($j=0,1,2$) yields $\xi_j=x$. So the error in the measured phase can be expressed in terms of $x$ and the exact phase $\alpha$:

$$\begin{aligned}\Delta\alpha(x,y) = {} & \left\{\frac{1}{2}\left(1-\frac{4x^2}{w_0^2}\right)(\cos\alpha-\sin\alpha)(1+\cos\alpha) - \frac{x}{2}\frac{d\alpha}{dx}\sin\alpha(\cos\alpha-\sin\alpha)\right\}\Delta\cos\theta_0 \\ & - \left\{\left(1-\frac{4x^2}{w_0^2}\right)\cos\alpha(1-\sin\alpha) - x\frac{d\alpha}{dx}\cos^2\alpha\right\}\Delta\cos\theta_1 \\ & + \left\{\frac{1}{2}\left(1-\frac{4x^2}{w_0^2}\right)(\cos\alpha+\sin\alpha)(1-\cos\alpha) + \frac{x}{2}\frac{d\alpha}{dx}\sin\alpha(\cos\alpha+\sin\alpha)\right\}\Delta\cos\theta_2\end{aligned} \qquad (3.23b)$$

From this expression the following upper bound for $|\Delta\alpha(x,y)|$ is deduced:

$$
\begin{aligned}
|\Delta\alpha(x,y)| \le\ & \frac{1}{2}\left|1-\frac{4x^2}{w_0^2}\right|\ |(\cos\alpha-\sin\alpha)(1+\cos\alpha)|\ |\Delta\cos\theta_0| \\
& + \left|\frac{x}{2}\right|\ \left|\frac{d\alpha}{dx}\right|\ |\sin\alpha(\cos\alpha-\sin\alpha)|\ |\Delta\cos\theta_0| \\
& + \left|1-\frac{4x^2}{w_0^2}\right|\ |\cos\alpha(1-\sin\alpha)|\ |\Delta\cos\theta_1| \\
& + |x|\ \left|\frac{d\alpha}{dx}\right|\ \cos^2\alpha\ |\Delta\cos\theta_1| \\
& + \frac{1}{2}\left|1-\frac{4x^2}{w_0^2}\right|\ |(\cos\alpha+\sin\alpha)(1-\cos\alpha)|\ |\Delta\cos\theta_2| \\
& + \left|\frac{x}{2}\right|\ \left|\frac{d\alpha}{dx}\right|\ |\sin\alpha(\cos\alpha+\sin\alpha)|\ |\Delta\cos\theta_2|
\end{aligned}
\tag{3.24}
$$

Averaging $|\Delta\alpha_m|$ over $\alpha$ under the assumption that $d\alpha/dx$ is independent of $\alpha$ gives:

$$
\begin{aligned}
|\Delta\alpha(x,y)|_{ave} \le\ & \frac{1}{2\pi}\left|1-\frac{4x^2}{w_0^2}\right|\ (2.83\,|\Delta\cos\theta_0| + 4\,|\Delta\cos\theta_1| + 2.83\,|\Delta\cos\theta_2|) \\
& + \frac{1}{2\pi}\ |x|\ \left|\frac{d\alpha}{dx}\right|\ (1.28\,|\Delta\cos\theta_0| + 3.2\,|\Delta\cos\theta_1| + 1.28\,|\Delta\cos\theta_2|)
\end{aligned}
\tag{3.25a}
$$

If it is further assumed that

$$
|\Delta\cos\theta_0| = |\Delta\cos\theta_1| = |\Delta\cos\theta_2| = |\Delta\cos\theta| \tag{3.26}
$$

equation (3.25a) simplifies to:

$$
|\Delta\alpha(x,y)|_{ave} \le 1.54\left|1-\frac{4x^2}{w_0^2}\right|\ |\Delta\cos\theta| + 1.076\,|x|\ \left|\frac{d\alpha}{dx}\right|\ |\Delta\cos\theta|
\tag{3.25b}
$$

An upper value is found by separate maximisation of the two terms on the right-hand side. The first term is maximum at the centre of the CCD-chip, i.e., at $x$=0. The second term is maximum at the border of the CCD-chip, i.e., at $x=w_0/2$. Under the assumption that the maximum gradient in $\alpha$ is $10^5 m^{-1}$ (see section 3.2) equation (3.25b) reduces to:

$$|\Delta\alpha|_{ave} \leq 324\,|\Delta\cos\theta| \qquad (3.25c)$$

Equation (3.25c) implies that if $\theta$ is smaller than 1.1° then $|\Delta\alpha|_{ave}$ will be smaller than 1% of $2\pi$. So if the angle between the normals of all three CCD-surfaces and the propagation direction of the beam is smaller than 1.1°, $|\Delta\alpha|_{ave}$ will be smaller than 1% of $2\pi$.

The maximal angle of 1.1° found for the rotation about the $y$-axis is valid for rotations about every axis in the CCD-surface through the origin. The reason is that by rotating the coordinate system about the propagation direction of the beam ($z$-axis), every axis can be described as $y$-axis while the analytical formalism remains the same. Compared to the required accuracy of 0.01° for rotation of the CCD-chip about the $z$-axis, a rotation accuracy of 1.1° is realized easily. The result, however, is only valid for the two lens imaging system. If the single lens imaging system is used, the beam is not parallel at the CCD-surface, so the intensity distribution will be more sensitive to $\theta$. This means that a smaller variation in $\theta$ is allowed while maintaining the same accuracy.

## 3.5 Conclusions

Each camera in a three camera interferometer has six degrees of freedom: translation along the $x$-axis, the $y$-axis and the $z$-axis and rotation about the $x$-axis, the $y$-axis and the $z$-axis. The alignment accuracy of these degrees of freedom is calculated under the assumption that the phase gradient of the beam at the position of the CCD-chips is smaller than $10^5 m^{-1}$.
The translational accuracies along the $x$-axis and the $y$-axis and the rotational accuracy about the $z$-axis are independent of the imaging system. The required translational accuracies are $\Delta x=\Delta y=0.5\mu m$. The required rotational accuracy is $\Delta\theta=0.01°$.
The translational accuracies along the $z$-axis and the rotational accuracy about the $x$-axis or the $y$-axis are dependent on the applied imaging system. The accuracies are much more critical for an interferometer equipped with a single lens imaging system than for an interferometer equipped with a two lens imaging system. Under the assumption that the test beam is still paraxial after passage through the test section, the required accuracy for the translation is 15$\mu$m and 2.4m, respectively. Despite the assumptions made in the derivation, the accuracies found here are a good first approximation. For an interferometer equipped with a two lens imaging system, a rotational accuracy of the CCD-chips about the $x$-axis or the $y$-axis of 1.1° is required. An interferometer equipped with a single lens imaging system requires a much better accuracy.

Because the translational accuracies of the CCD-chips along the $z$-axis and the rotational accuracy about the $x$-axis or the $y$-axis are less critical, a two lens imaging system is preferred to a single lens imaging system. When using the two lens imaging system, not only the translational accuracy of the CCD-chips along the $z$-axis is not critical, but also the rotational accuracy about the $x$-axis and the $y$-axis are not critical when compared to the required rotational accuracy about the $z$-axis. In a practical set-up these accuracies can be realized easily. So it can be concluded that in an interferometer with a two lens imaging system instead of a single lens imaging system, the number of degrees of freedom per camera is only three instead of six.

The accuracies mentioned above are based on a maximum average modulus of the error in the measured phase ($|\Delta\alpha|_{ave}$) of 1% of $2\pi$. They were calculated under the assumption that the CCD-cameras are perfectly aligned in all degrees of freedom, except the degree(s) of freedom under study. When all degrees of freedom of the CCD-cameras are adjusted with the mentioned accuracy, the total value of $|\Delta\alpha|_{ave}$ is 4% of $2\pi$: 1% due to the limited translational accuracy along the $x$-axis and the $y$-axis, 1% due to the limited rotational accuracy about the $z$-axis, 1% for the limited translational accuracy along the $z$-axis and 1% due to the limited rotational accuracy about the $x$-axis or the $y$-axis. This value excludes phase errors due to misalignment of the quarter wave plate and the polariser in front of CCD1 as well as phase errors due to the limited accuracy in the normalization of the intensity levels on the CCD-chip.

# 4. Alignment accuracies of the quarter wave plate and the polariser

## 4.1 Introduction

The detection system of an interferometer with three cameras is shown in figure 4.1. The electric field of the beam entering the system contains two rectangular polarisation components. Component $\boldsymbol{E}_t(t)$, polarised in the $x$-direction, is the electric field of the interferometer's test beam. Due to the passage through the test section it is shifted in phase over $\alpha$. Component $\boldsymbol{E}_r(t)$, polarised in the $y$-direction, is the electric field of the interferometer's reference beam. A quarter wave plate R3, whose fast axis is at 45° to the $x$-axis, transforms the rectangular linear polarisation states of $\boldsymbol{E}_t(t)$ and $\boldsymbol{E}_r(t)$ into opposite circular polarisation states. In this beam the phase difference between $\boldsymbol{E}_t(t)$ and $\boldsymbol{E}_r(t)$ can be selected easily, because an extra phase shift can be introduced to the phase shift $\alpha$. This extra phase shift is dependent on the linear polarisation direction which is transmitted by the optical components in the set-up. The opposite circularly polarised beam is split by beamsplitter BS. The transmitted beam is next split by the polarising beamsplitter PBS1. The $x$-polarised light, i.e., the $x$-components of $\boldsymbol{E}_t(t)$ and $\boldsymbol{E}_r(t)$, is transmitted to CCD0. The $y$-polarised light, i.e., the $y$-components of $\boldsymbol{E}_t(t)$ and $\boldsymbol{E}_r(t)$, is reflected to CCD2. The beam reflected by beamsplitter BS passes a piece of glass (to compensate for the fact that the transmitted beam passes the polarising beamsplitter cube PBS1) and a polariser whose transmission axis is at 45° to the $x$-axis. So the light reaching CCD1 is linearly polarised at 45° to the $x$-axis. Due to the different polarisation directions of the light on the three CCD-chips, the phase difference between $\boldsymbol{E}_t(t)$ and $\boldsymbol{E}_r(t)$ differs for each camera. In the $x$-polarised beam on CCD0, an extra phase shift of $\pi/2$ is introduced in $\boldsymbol{E}_r(t)$ relative to $\boldsymbol{E}_t(t)$. Because $\boldsymbol{E}_t(t)$ is shifted in phase over $\alpha$ due to the passage through the test section, the total phase difference between $\boldsymbol{E}_t(t)$ and $\boldsymbol{E}_r(t)$ is equal to $\alpha-\pi/2$. Similarly, in the $y$-polarised beam on CCD2 an extra phase shift of $\pi/2$ is introduced to $\boldsymbol{E}_t(t)$ relative to $\boldsymbol{E}_r(t)$, so the total phase difference is $\alpha+\pi/2$. In the beam on CCD1, polarised at 45° to the

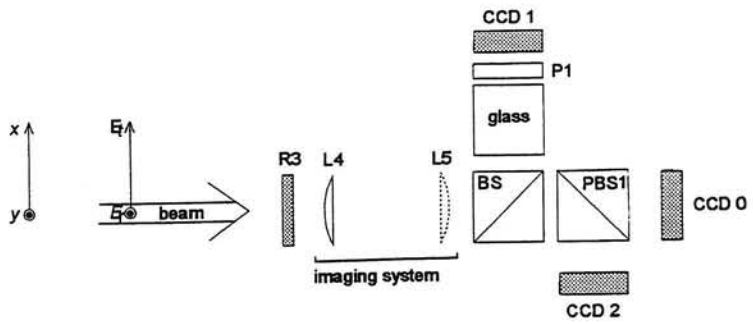


**Figure 4.1** The three camera detection system. The symbols are from figure 2.2.

$x$-axis, $\boldsymbol{E}_t(t)$ and $\boldsymbol{E}_r(t)$ are not shifted in phase relative to each other, so the phase difference is $\alpha$. The phase shift between $\boldsymbol{E}_t(t)$ and $\boldsymbol{E}_r(t)$ on a CCD-chip is equal to the phase of the interference pattern on the CCD-chip. This implies that the interference pattern on CCD2 is shifted in phase over $\pi$ compared to the interference pattern on CCD0. Similarly, the interference pattern on CCD1 is shifted in phase over $\pi/2$ compared to the interference pattern on CCD0.

In the set-up, beside the CCD-cameras four optical components have to be aligned: the quarter wave plate, the non-polarising beamsplitter, the polariser and the polarising beamsplitter. The depolarisation rate of the beams leaving the polarising beamsplitter is negligible and the polarisation directions are perpendicular, so this element is easily aligned. The non-polarising beamsplitter, however, is not ideal: transmission and reflection are not independent of the polarisation state. This will influence the measured phase $\alpha$, just as small errors in the orientation of the quarter wave plate and the polariser will do.

In this section the error in $\alpha$ due to a misalignment of the quarter wave plate and the polariser will be analysed. The errors in $\alpha$ due to the polarisation dependency of the non-polarising beamsplitter can be corrected in an optical way. Attention will be paid to the questions how to make this correction and how this correction influences the required normalization of the intensity distributions on the three cameras.

## 4.2 Phase error calculation

In this section an analytical expression will be derived for the intensity distributions on CCD0, CCD1 and CCD2 as a function of the orientation of the quarter wave plate, the orientation of the polariser and the transmission/reflection coefficient of the non-polarising beamsplitter.

In figure 4.1 the output beam of the interferometer enters the detection system. The beam contains two components: the $x$-polarised test beam with electric field amplitude $E_t$ and the $y$-polarised reference beam with electric field amplitude $E_r$. The total electric field vector $\boldsymbol{E}_{xy}$ can be written as:

$$\boldsymbol{E}_{xy} = \begin{bmatrix} E_t e^{-i\alpha} \\ E_r \end{bmatrix} \tag{4.1}$$

where the time dependence has been omitted for notational simplicity. The subscript $xy$ refers to the Cartesian coordinate system $(x,y)$ to which the vector is attached. This electric field passes a quarter wave plate whose fast axis is oriented at $(45\text{-}\phi)^\circ$ to the $x$-axis, see figure 4.2. In figure 4.3 a new Cartesian coordinate system $(x',y')$ is defined. The origin of this coordinate system coincides with the origin of the coordinate system $(x,y)$.

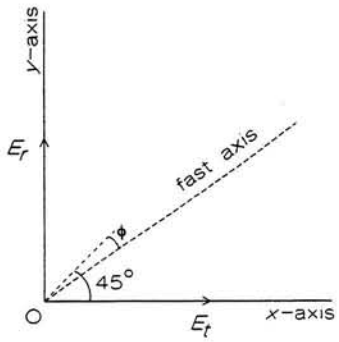


**Figure 4.2** The orientation of the quarter wave plate's fast axis in the electric field of the interferometer in the ideal situation and in the actual situation.

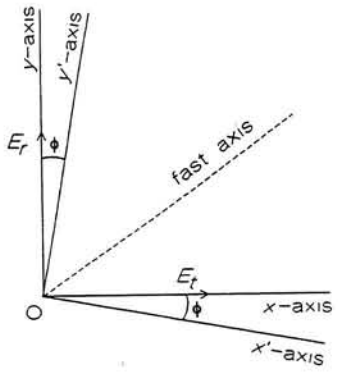


**Figure 4.3** Definition of the coordinate system (x'y') compared to the coordinate system (x,y) and the fast axis of the quarter wave plate.

However, the coordinate system $(x',y')$ is rotated over an angle $\phi$ about the origin. So the fast axis of the quarter wave plate is at 45° to the $x'$-axis. The electric field of equation (4.1) expressed in these coordinates, $\boldsymbol{E}_{x'y'}$, is:

$$\boldsymbol{E}_{x'y'} = \begin{bmatrix} \cos\phi & -\sin\phi \\ \sin\phi & \cos\phi \end{bmatrix} \begin{bmatrix} E_t e^{-i\alpha} \\ E_r \end{bmatrix} = \begin{bmatrix} E_t\cos\phi\, e^{-i\alpha} - E_r\sin\phi \\ E_t\sin\phi\, e^{-i\alpha} + E_r\cos\phi \end{bmatrix} \tag{4.2}$$

When the electric field has passed the quarter wave plate, it is equal to:[3,4]

$$\boldsymbol{E}_{x'y'} = \frac{1}{\sqrt{2}} \begin{bmatrix} 1 & -i \\ -i & 1 \end{bmatrix} \begin{bmatrix} E_t\cos\phi\, e^{-i\alpha} - E_r\sin\phi \\ E_t\sin\phi\, e^{-i\alpha} + E_r\cos\phi \end{bmatrix} = \frac{1}{\sqrt{2}} \begin{bmatrix} E_t e^{-i(\phi+\alpha)} - iE_r e^{-i\phi} \\ -iE_t e^{i(\phi-\alpha)} + E_r e^{i\phi} \end{bmatrix} \tag{4.3}$$

Transformation to the coordinate system $(x,y)$ gives:

$$\begin{aligned} \boldsymbol{E}_{xy} &= \frac{1}{\sqrt{2}} \begin{bmatrix} \cos\phi & \sin\phi \\ -\sin\phi & \cos\phi \end{bmatrix} \begin{bmatrix} E_t e^{-i(\phi+\alpha)} - iE_r e^{-i\phi} \\ -iE_t e^{i(\phi-\alpha)} + E_r e^{i\phi} \end{bmatrix} \\ &= \frac{1}{\sqrt{2}} \begin{bmatrix} E_t\cos\phi\, e^{-i(\phi+\alpha)} - iE_r\cos\phi\, e^{-i\phi} - iE_t\sin\phi\, e^{i(\phi-\alpha)} + E_r\sin\phi\, e^{i\phi} \\ -E_t\sin\phi\, e^{-i(\phi+\alpha)} + iE_r\sin\phi\, e^{-i\phi} - iE_t\cos\phi\, e^{i(\phi-\alpha)} + E_r\cos\phi\, e^{i\phi} \end{bmatrix} \end{aligned} \tag{4.4}$$

Next the beam is split by a non-polarising beamsplitter BS, whose power reflection

coefficient is $a$ for $x$-polarised light and $b$ for $y$-polarised light. The transmitted beam is split again by the polarising beam splitter. The power transmission coefficient of this beamsplitter is 1 for $x$-polarised light. The power reflection coefficient is 1 for $y$-polarised light. So the electric field $E_0$ on CCD0 is $x$-polarised and is given by:

$$E_0 = \sqrt{\frac{1-a}{2}}\,(E_t\cos\phi e^{-i(\phi+\alpha)} - iE_r\cos\phi e^{-i\phi} - iE_t\sin\phi e^{i(\phi-\alpha)} + E_r\sin\phi e^{i\phi}) \tag{4.5a}$$

The electric field $E_2$ on CCD2 is $y$-polarised and is given by:

$$E_2 = \sqrt{\frac{1-b}{2}}\,(-E_t\sin\phi e^{-i(\phi+\alpha)} + iE_r\sin\phi e^{-i\phi} - iE_t\cos\phi e^{i(\phi-\alpha)} + E_r\cos\phi e^{i\phi}) \tag{4.5b}$$

For the electric field vector $\boldsymbol{E}_{\rho,xy}$ between the non-polarising beamsplitter and the polariser follows:

$$\boldsymbol{E}_{\rho,xy} = \frac{1}{\sqrt{2}}\begin{bmatrix}\sqrt{a}\,(E_t\cos\phi e^{-i(\phi+\alpha)} - iE_r\cos\phi e^{-i\phi} - iE_t\sin\phi e^{i(\phi-\alpha)} + E_r\sin\phi e^{i\phi}) \\ \sqrt{b}\,(-E_t\sin\phi e^{-i(\phi+\alpha)} + iE_r\sin\phi e^{-i\phi} - iE_t\cos\phi e^{i(\phi-\alpha)} + E_r\cos\phi e^{i\phi})\end{bmatrix} \tag{4.5c}$$

Behind the polariser whose transmission axis is oriented at an angle $\theta$ to the $x$-axis, the electric field $E_1$ is given by:

$$\begin{aligned} E_1 = {} & \sqrt{\frac{a}{2}}\,(E_t\cos\phi e^{-i(\phi+\alpha)} - iE_r\cos\phi e^{-i\phi} - iE_t\sin\phi e^{i(\phi-\alpha)} + E_r\sin\phi e^{i\phi})\cos\theta \\ & + \sqrt{\frac{b}{2}}\,(-E_t\sin\phi e^{-i(\phi+\alpha)} + iE_r\sin\phi e^{-i\phi} - iE_t\cos\phi e^{i(\phi-\alpha)} + E_r\cos\phi e^{i\phi})\sin\theta \end{aligned} \tag{4.5d}$$

This is the electric field on CCD1. The polarisation direction of this linearly polarised field is at an angle $\theta$ to the $x$-axis. The intensity distributions $I_0$, $I_1$, $I_2$ on CCD0, CCD1 and CCD2 can easily be calculated by multiplying the electric fields with their complex conjugates:

$$I_0 \propto E_0 E_0^*$$

$$= \frac{1-a}{2}\left(E_t^2 + E_r^2 + 2E_t E_r \cos 2\phi \cos(\alpha - \frac{\pi}{2}) + (E_t^2 - E_r^2)\sin^2 2\phi + E_t E_r \sin 4\phi \cos\alpha\right) \tag{4.6a}$$

$$I_2 \propto E_2 E_2^*$$

$$= \frac{1-b}{2}\left(E_t^2 + E_r^2 + 2E_t E_r \cos 2\phi \cos(\alpha + \frac{\pi}{2}) - (E_t^2 - E_r^2)\sin^2 2\phi - E_t E_r \sin 4\phi \cos\alpha\right) \tag{4.6b}$$

$$I_1 \propto E_1 E_1^*$$

$$= \frac{a\cos^2\theta}{1-a} E_0 E_0^* + \frac{b\sin^2\theta}{1-b} E_2 E_2^*$$

$$+ \sqrt{ab}\cos\theta \sin\theta\left(2E_t E_r(\cos^2 2\phi \cos\alpha - \sin 2\phi \sin\alpha) + \frac{1}{2}(E_t^2 - E_r^2) sin4\phi\right) \tag{4.6c}$$

If the quarter wave plate is aligned perfectly, i.e., $\phi = 0^0$, the expressions for the intensity distributions on CCD0, CCD2 and CCD1 reduce to:

$$I_0 \propto E_0 E_0^* = \frac{1-a}{2}\left(E_t^2 + E_r^2 + 2E_t E_r \cos(\alpha - \frac{\pi}{2})\right) \tag{4.7a}$$

$$I_2 \propto E_2 E_2^* = \frac{1-b}{2}\left(E_t^2 + E_r^2 + 2E_t E_r \cos(\alpha + \frac{\pi}{2})\right) \tag{4.7b}$$

$$I_1 \propto E_1 E_1^* = \frac{a\cos^2\theta}{1-a} E_0 E_0^* + \frac{b\sin^2\theta}{1-b} E_2 E_2^* + \sqrt{ab}\cos\theta \sin\theta\left(2E_t E_r \cos\alpha\right) \tag{4.7c}$$

To realize a modulation of $I_1$ which is independent of $\cos(\alpha - \pi/2)$ and $\cos(\alpha + \pi/2)$ terms, these terms should cancel in equation (4.7c). This will be the case if the next condition is fulfilled:

$$a\cos^2\theta = b\sin^2\theta \tag{4.8}$$

$I_1$ can now be written as:

$$I_1 \propto a\cos^2\theta\left(E_t^2 + E_r^2 + 2E_tE_r\cos\alpha\right) \tag{4.7d}$$

Requirement (4.8) implies that for the situation $a$ is equal to $b$, $\theta$ has to be 45°. In practice, however, $a$ is unequal to $b$, so $\theta$ has to be unequal to 45°.

Equations (4.7a), (4.7b) and (4.7d) show a phase shift of $-\pi/2$ in the intensity distributions $I_j$ compared to equation (3.3b). This means that substitution of these values of $I_0$, $I_1$ and $I_2$ in equation (3.4a) will also lead to a value for $\alpha$ which is shifted over $-\pi/2$. So if the intensities defined in equations (4.7a), (4.7b) and (4.7d) are used, the correct value for $\alpha$ is:

$$\alpha(x,y) = \arctan\left(\frac{\kappa_2 I_2 - \kappa_1 I_1}{\kappa_0 I_0 - \kappa_1 I_1}\right) - \frac{\pi}{4} \tag{4.9}$$

In this equation $\kappa_0$, $\kappa_1$, and $\kappa_2$ are normalization factors. If the sensitivity is the same for all cameras, it is easy to see with equations (4.7a), (4.7b) and (4.7d) that:

$$\kappa_0 = \frac{2}{1-a} \tag{4.10a}$$

$$\kappa_1 = \frac{1}{a\cos^2\theta} \tag{4.10b}$$

$$\kappa_2 = \frac{2}{1-b} \tag{4.10c}$$

The non-polarising beamsplitter in the set-up of figure 4.1 is characterised by $a$=0.45 and $b$=0.65. So for exact phase measurements the required exact values for $\theta$, $\phi$, $\kappa_0$, $\kappa_1$ and $\kappa_2$ are: $\theta$=0.694 rad (39.76°), $\phi$=0 rad, $\kappa_0$=3.64, $\kappa_1$=3.76 and $\kappa_2$=5.71. However, in a practical set-up it is difficult to adjust $\theta$ and $\phi$ exactly. So it is important to know the absolute error in $\alpha$ if $\theta$ is not exactly equal to 0.694 rad and $\phi$ is not exactly equal to 0 rad, while for $\kappa_0$, $\kappa_1$ and $\kappa_2$ the exact values are used. Under the assumption $E_t$=$E_r$ these errors are calculated by using equations (4.6a), (4.6b), (4.6c) and (4.8). Figure 4.4 shows the phase error $\Delta\alpha$ when $\theta$=0.694 rad and $\phi$=0.017 rad (1°), i.e., $\theta$ has its exact value and $\phi$ is shifted over 1° compared to its exact value. Figure 4.5 shows the phase error $\Delta\alpha$ when $\theta$=0.711 rad (46°) and $\phi$=0 rad, i.e., $\theta$ is shifted over 1° compared to its exact value and $\phi$

has its exact value. Figure 4.6a,b shows the modulus of $\Delta\alpha$ averaged over $\alpha$ ($|\Delta\alpha|_{ave}$) as a function of $\phi$ when $\theta$=0.694 rad (exact value). If the system is aligned exactly, $|\Delta\alpha|_{ave}$ is independent of the quotient $E_t/E_r$. However, if the system is not aligned exactly $|\Delta\alpha|_{ave}$ is not independent of this quotient. So in figure 4.6a,b $|\Delta\alpha|_{ave}$ is represented as a function of $\phi$ for $E_t/E_r$=1, $E_t/E_r$=1.25 and $E_t/E_r$=10. Figure 4.7a,b shows $|\Delta\alpha|_{ave}$ as a function of $\theta$ for $E_t/E_r$=1, $E_t/E_r$=1.25 and $E_t/E_r$=10, when $\phi$=0 rad (exact value).

Inverting the quotient $E_t/E_r$ does not change $|\Delta\alpha|_{ave}$ as function of $\phi$ when $\theta$, $\kappa_0$, $\kappa_1$, and $\kappa_2$ have their exact value. Similarly, inverting $E_t/E_r$ does not change $|\Delta\alpha|_{ave}$ as function of $\theta$ for $\phi$=0, no matter what the values of $\kappa_0$, $\kappa_1$, and $\kappa_2$ are. This is easy to see if one realizes that:

$$|\Delta\alpha|_{ave} = \left\langle \left| \arctan\left(\frac{\kappa_2 I_2 - \kappa_1 I_1}{\kappa_0 I_0 - \kappa_1 I_1}\right) - \frac{\pi}{4} - \alpha \right| \right\rangle \tag{4.11a}$$

For the first situation, the argument of the arctangent function can be written as:

$$\frac{\kappa_2 I_2 - \kappa_1 I_1}{\kappa_0 I_0 - \kappa_1 I_1} = \frac{c_1(E_t^2 - E_r^2) + c_2 E_t E_r \cos\alpha + c_3 E_t E_r \sin\alpha}{c_4(E_t^2 - E_r^2) + c_5 E_t E_r \cos\alpha + c_6 E_t E_r \sin\alpha} \tag{4.11b}$$

where $c_i$ (i=1,2,3,4,5,6) are functions of $\phi$. In the second situation the argument can be written as:

$$\frac{\kappa_2 I_2 - \kappa_1 I_1}{\kappa_0 I_0 - \kappa_1 I_1} = \frac{f_1(E_t^2 + E_r^2) + f_2 E_t E_r \sin\alpha + f_3 E_t E_r \cos\alpha}{f_4(E_t^2 + E_r^2) + f_5 E_t E_r \sin\alpha + f_6 E_t E_r \cos\alpha} \tag{4.11c}$$

where $f_i$ are functions of some of the parameters $\theta$, $\kappa_0$, $\kappa_1$ and $\kappa_2$. Substituting the two arguments in equation (4.11a) and averaging over $\alpha$ give the same result for the case that the quotient is $E_t/E_r$ and the case the quotient is inverted.

Figure 4.8a shows $|\Delta\alpha|_{ave}$ as a function of $\kappa_0$ with free parameter $E_t/E_r$. The values of $\kappa_1$, $\kappa_2$, $\theta$ and $\phi$ have their exact values. Similarly figure 4.8b and 4.8c show $|\Delta\alpha|_{ave}$ as function of $\kappa_1$ and $\kappa_2$ when $\kappa_0$, $\theta$ and $\phi$ have their exact values, just as $\kappa_2$ and $\kappa_1$ respectively. Also here inverting $E_t/E_r$ will not lead to a change in $|\Delta\alpha|_{ave}$.

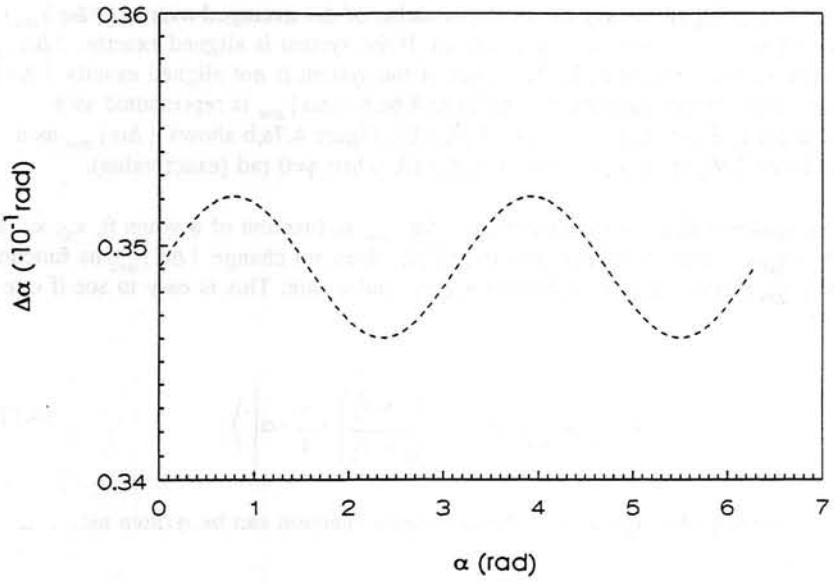


**Figure 4.4** The absolute phase error $\Delta\alpha$ as a function of the phase $\alpha$ when $\theta$ has its exact value 0.694 rad and $\phi$ is equal to 0.017 rad.

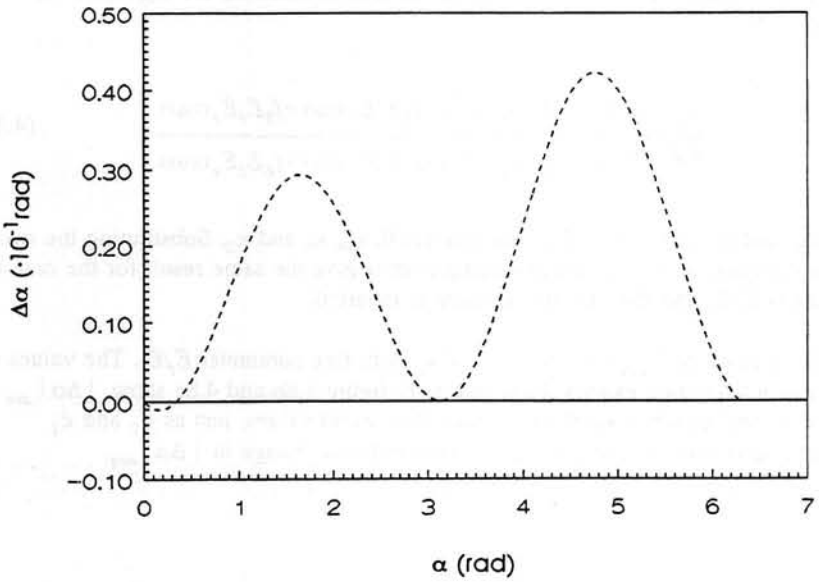


**Figure 4.5** The absolute phase error $\Delta\alpha$ as a function of the phase $\alpha$ when $\theta$ is equal to 0.711 rad and $\phi$ has its exact value 0 rad.

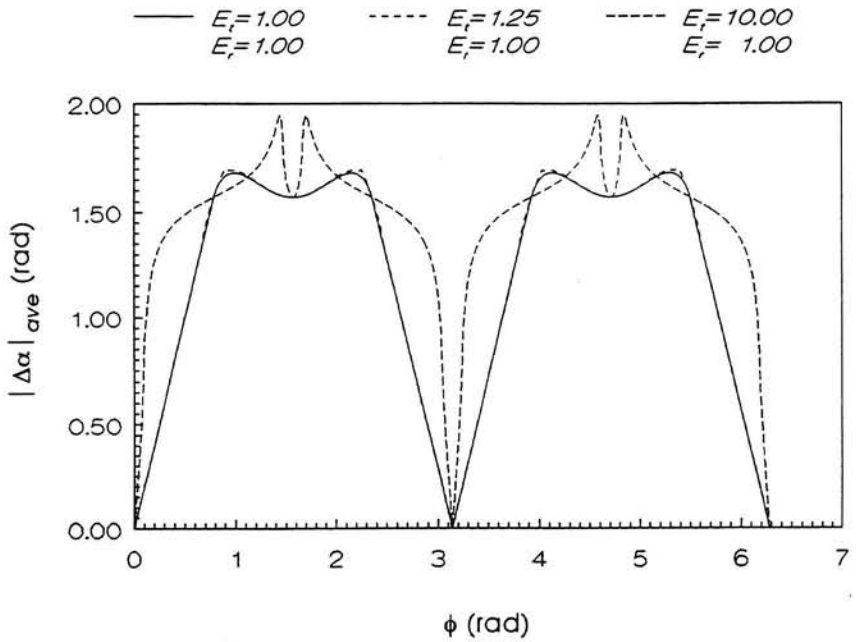


a.

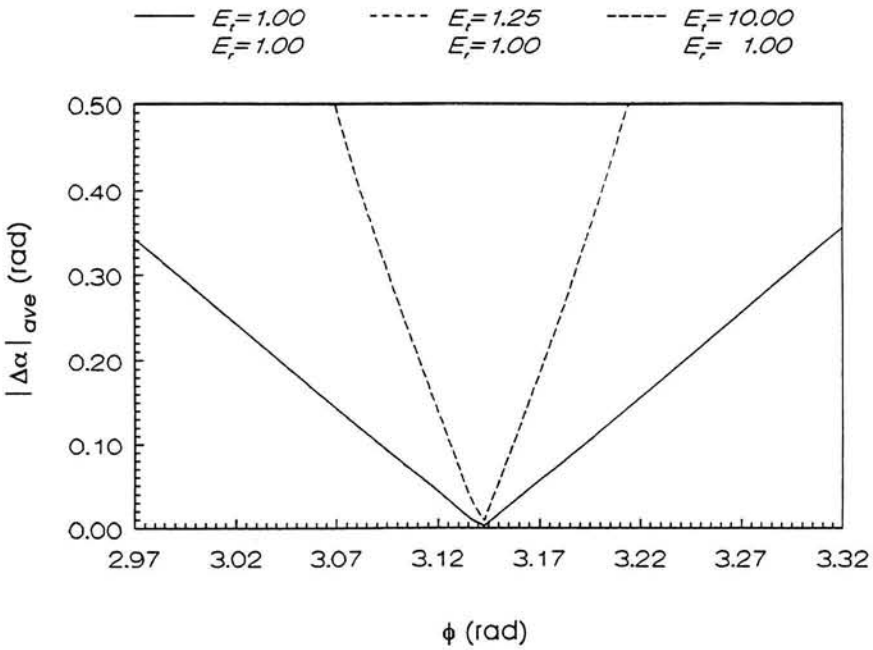


b.

**Figure 4.6a,b** The average modulus of the phase error $|\Delta\alpha|_{ave}$ as a function of $\phi$ with free parameter $E_t/E_r$. The other parameters are exact.

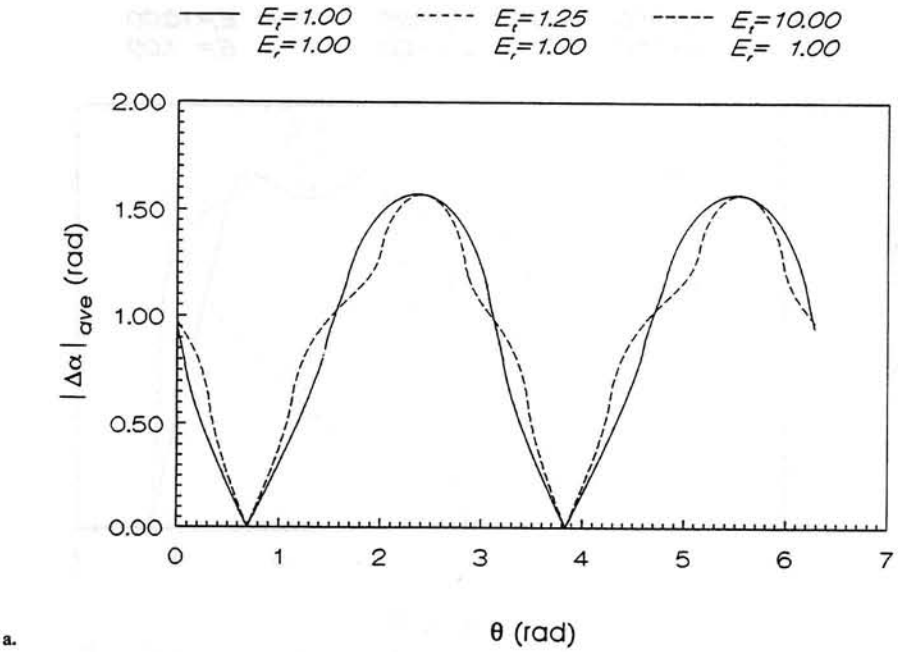


a.

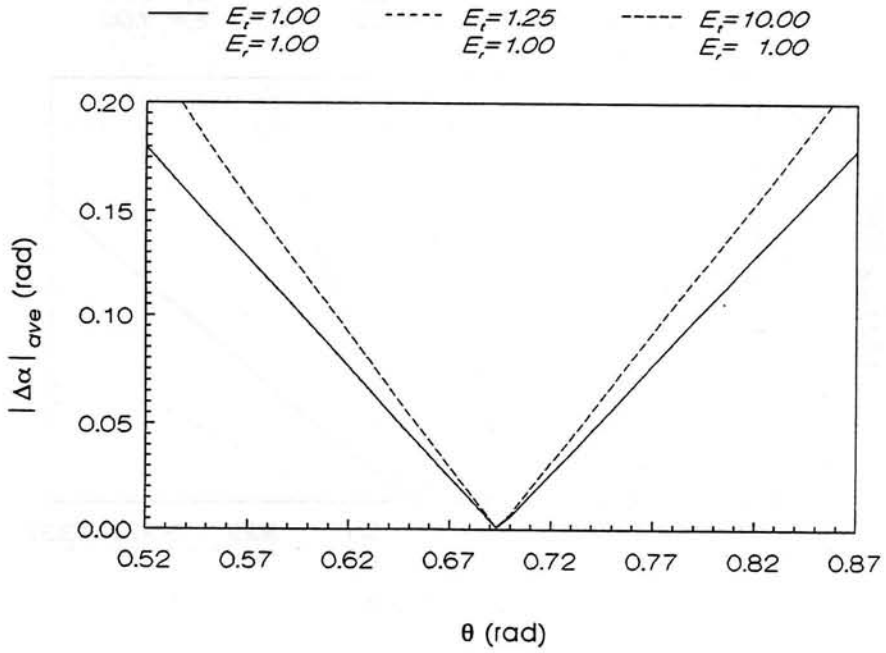


b.

**Figure 4.7a,b** The average modulus of the phase error $|\Delta\alpha|_{ave}$ as a function of θ with free parameter $E_t/E_r$. The other parameters are exact.

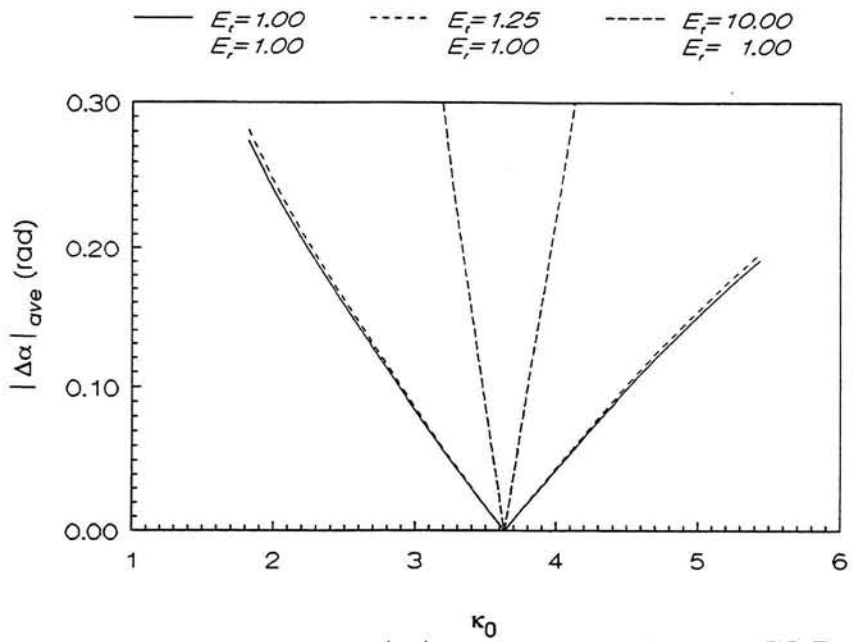


**Figure 4.8a** The average modulus of the phase error $|\Delta\alpha|_{ave}$ as a function of $\kappa_0$ with free parameter $E_t/E_r$. The other parameters are exact.

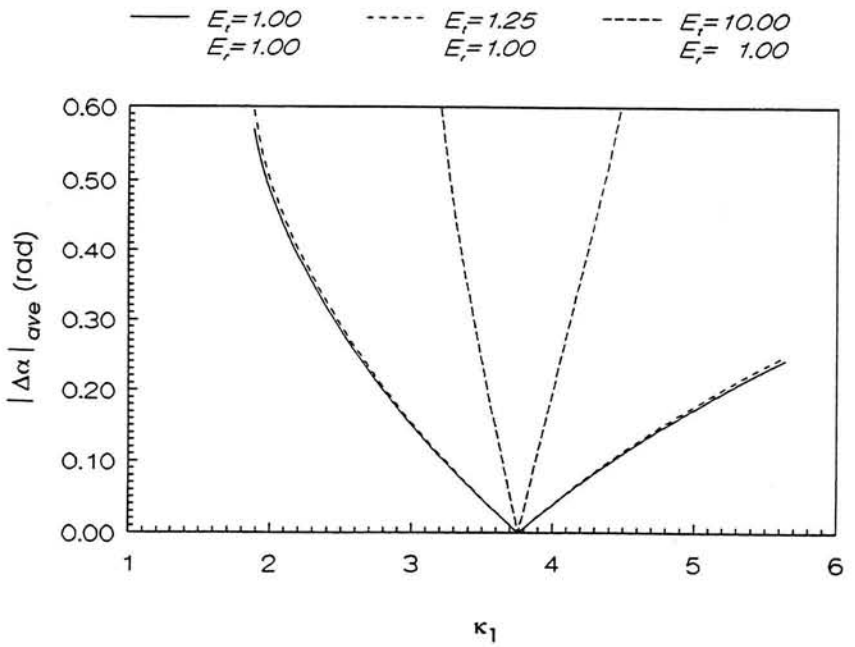


**Figure 4.8b** The average modulus of the phase error $|\Delta\alpha|_{ave}$ as a function of $\kappa_1$ with free parameter $E_t/E_r$. The other parameters are exact.

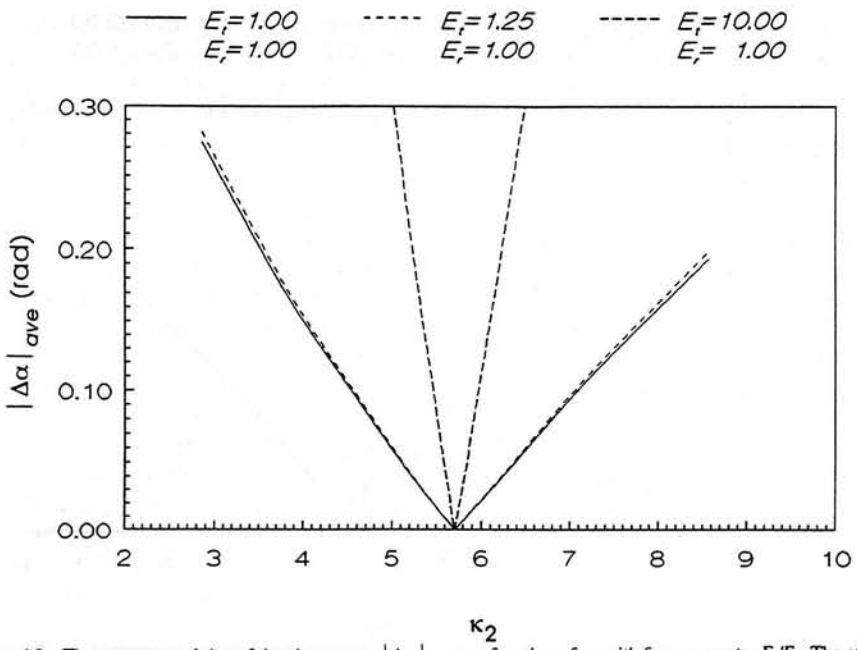


**Figure 4.8c** The average modulus of the phase error $|\Delta\alpha|_{ave}$ as a function of $\kappa_2$ with free parameter $E_t/E_r$. The other parameters are exact.

### 4.3 Discussion and conclusions

To evaluate the results of section 4.2 some new parameters are introduced: $\Delta\phi$, $\Delta\theta$, $\Delta\kappa_0$, $\Delta\kappa_1$ and $\Delta\kappa_2$. These parameters are equal to the modulus of the difference between the exact and the actual values of the parameters $\phi$, $\theta$, $\kappa_0$, $\kappa_1$ and $\kappa_2$, respectively:

$$\Delta\phi = |\phi| \tag{4.12a}$$

$$\Delta\theta = |0.694-\theta| \tag{4.12b}$$

$$\Delta\kappa_0 = \left|\frac{2}{1-a}-\kappa_0\right| \tag{4.12c}$$

$$\Delta\kappa_1 = \left|\frac{1}{0.591a}-\kappa_1\right| \tag{4.12d}$$

$$\Delta\kappa_2 = \left|\frac{2}{1-b}-\kappa_2\right| \tag{4.12e}$$

Figure 4.6a shows that the error in the average modulus of $\alpha$ is a periodic function of $\phi$ with period $\pi$. This is easy to understand, because after rotating the quarter wave plate over an angle $\pi$, the fast and slow axis of the crystal obtain their original directions again. Similarly, the average modulus of the error in $\alpha$ as a function of $\theta$ is periodic with period $\pi$ (see figure 4.7a): after rotating the polariser over an angle $\pi$, the transmission axis obtains its original direction again.

Figure 4.6a shows that for $\phi=k\pi$ (k=0,1,2..) the measured phase $\alpha$ is correct, independent of $E_t/E_r$. For small values of $\Delta\phi$ there exists an almost linear relation between $|\Delta\alpha|_{ave}$ and $\Delta\phi$, see figure 4.6b. When $E_t/E_r=1$ and $\Delta\phi<0.8$ rad ($\approx 45^\circ$) this relation can be approximated by: $|\Delta\alpha|_{ave}/\Delta\phi\approx 2.08$. If an average error in $\alpha$ of 1% of $2\pi$ due to misalignment of $\phi$ is allowed, the accuracy to which the quarter wave plate has to be adjusted is $\Delta\phi=0.03$ rad ($1.7^\circ$). The relation between $|\Delta\alpha|_{ave}$ and $\phi$ almost does not change when $E_t/E_r$ increases from 1 to 1.25. However, if $E_t/E_r$ increases to 10 the relation changes and $|\Delta\alpha|_{ave}/\Delta\phi$ for small $\Delta\phi$ also increases strongly.
Similarly, figure 4.7a,b shows that $|\Delta\alpha|_{ave}$ is zero for $\theta=0.694\pm k\pi$ (k=0,1,2...), independent of $E_t/E_r$. For small values of $\Delta\theta$, the relation between $|\Delta\alpha|_{ave}$ and $\Delta\theta$ is almost linear. When $E_t/E_r=1$ and $\Delta\theta<0.4$ rad ($\approx 23^\circ$) this relation is: $|\Delta\alpha|_{ave}/\Delta\theta\approx 1.03$. So to keep the error smaller than 1% of $2\pi$, it is required that $\Delta\theta<0.06$ rad ($3.5^\circ$). Increasing $E_t/E_r$ to 1.25 almost does not change $|\Delta\alpha|_{ave}$ as function of $\theta$. However, increasing $E_t/E_r$ to 10 changes the curve strongly.

The relation between $|\Delta\alpha|_{ave}$ and the normalization factor $\kappa_i$ (i=0,1,2) is almost linear for small $\Delta\kappa_i$ when all other parameters (including the other normalization factors) have their exact values, see figure 4.8a,b,c. This relation is almost the same for $E_t/E_r=1$ and $E_t/E_r=1.25$. For $E_t/E_r=10$, however, $|\Delta\alpha|_{ave}/\Delta\kappa_i$ increases. To keep $|\Delta\alpha|_{ave}$ smaller than 1% of $2\pi$ when $E_t/E_r=1$, it is required that:

$$3.16 < \kappa_0 < 4.16 \qquad (4.13a)$$

$$3.42 < \kappa_1 < 4.16 \qquad (4.13b)$$

$$4.97 < \kappa_2 < 6.54 \qquad (4.13c)$$

This implies that $\kappa_0$ and $\kappa_2$ are allowed to be 13% smaller and 14.5% larger than the exact values 3.64 and 5.71, respectively. $\kappa_1$ is allowed to be 9% smaller and 10.5% larger than the exact value 3.76. The linear relation between $|\Delta\alpha|_{ave}$ and $\Delta\kappa_i$ is given by:

$$\frac{|\Delta\alpha|_{ave}}{\Delta\kappa_0} = 0.13 \quad (\kappa_0<3.64) \qquad (4.14a)$$

$$\frac{|\Delta\alpha|_{ave}}{\Delta\kappa_0} = 0.12 \quad (\kappa_0>3.64) \qquad (4.14b)$$

$$\frac{|\Delta\alpha|_{ave}}{\Delta\kappa_1} = 0.18 \quad (\kappa_1<3.76) \tag{4.14c}$$

$$\frac{|\Delta\alpha|_{ave}}{\Delta\kappa_1} = 0.16 \quad (\kappa_1>3.76) \tag{4.14d}$$

$$\frac{|\Delta\alpha|_{ave}}{\Delta\kappa_2} = 0.082 \quad (\kappa_2<5.71) \tag{4.14e}$$

$$\frac{|\Delta\alpha|_{ave}}{\Delta\kappa_2} = 0.075 \quad (\kappa_2>5.71) \tag{4.14f}$$

The theoretical derivations in section 4.2 and the discussion in this section lead to the following conclusions for a three camera interferometer, with a non-polarising beamsplitter that is characterised by $a$=0.45 and $b$=0.65:

- For a correct phase measurement the parameters $\phi$, $\theta$, $\kappa_0$, $\kappa_1$, and $\kappa_2$ have to be equal to their exact values: $\phi=0°$, $\theta=39.76°$, $\kappa_0=3.64$, $\kappa_1=3.76$, $\kappa_2=5.71$.
- Increasing $E_t/E_r$ from 1 to 1.25 almost does not influence $|\Delta\alpha|_{ave}$, so a difference between the electric field of the reference beam and the test beam of 25% is allowed.
- If all parameters have their exact values except one, the allowed variation in this parameter while keeping $|\Delta\alpha|_{ave}$ smaller than 1% of $2\pi$, is: $\Delta\phi<1.7°$, $\Delta\theta<3.5°$, $\Delta\kappa_0<0.48$ (13% of the exact value for $\kappa_0$), $\Delta\kappa_1<0.34$ (9% of the exact value for $\kappa_1$), $\Delta\kappa_2<0.74$ (13% of the exact value for $\kappa_2$).
- There exists a complex relation between the different parameter errors and $|\Delta\alpha|_{ave}$. However, to a first approximation the total error $|\Delta\alpha|_{ave}$ due to a combination of errors in $\phi$, $\theta$, $\kappa_0$, $\kappa_1$ and $\kappa_2$ will be the sum of the errors $|\Delta\alpha|_{ave}$ due to the errors in the individual parameters. So if the parameters are adjusted with the accuracy as described here, the maximal total error $|\Delta\alpha|_{ave}$ amounts to about 5% of $2\pi$.

These conclusions are the result of an analysis in which the errors due to a misalignment of the CCD-chips were excluded. Chapter 3 has shown that if the alignment of the CCD-chips satisfies the required accuracy, $|\Delta\alpha|_{ave}$ due to the misalignment of the CCD-chips is less than 4% of $2\pi$. This value of $|\Delta\alpha|_{ave}$ has to be added to the value of 5% of $2\pi$ found in this section. So the total estimated error in $\alpha$, $|\Delta\alpha|_{ave}$, is equal to 9% of $2\pi$.

# 5. Summarized conclusions.

A Michelson interferometer for quantitative refractive index measurements has been designed. A Michelson interferometer is preferred to a Mach Zehnder interferometer because it is easier to install around large objects like a wind tunnel. This report is a theoretical analysis of the interferometer and treats two major subjects:

1. The choice between a two and a three camera interferometer.
2. The required alignment accuracy of the elements in the interferometer as well as the required accuracy in the normalization factors.

Ad 1.

A three camera interferometer is preferred to a two camera system because:

- the range in which the phase shift can be detected is $0\text{-}2\pi$ for a three camera interferometer and $0\text{-}\pi$ for a two camera interferometer,
- the two camera interferometer is less sensitive to spatial low frequency phase variations,
- the two camera interferometer introduces more undesired intensity fluctuations due to a rotating inhomogeneous quarter wave plate.
- the sampling moments at which the phase is measured have to be known exactly when using the two camera interferometer.

Ad 2.

A three camera interferometer equipped with a two lens imaging system is preferred to a interferometer equipped with a single lens imaging system. The two lens system reduces the degrees of freedom of the CCD-camera's from 6 to 3 per camera. If the maximum phase gradient in the image on the CCD-chips is $10^5$ rad/m, the total average modulus of the error in the measured phase can be kept smaller than 9% of $2\pi$. This error excludes errors due to refraction effects in the examined medium in the test section. For an interferometer equipped with a two lens imaging system, the required alignment accuracy for the optical components is given by:

CCD-cameras:
$x,y$ translation: 0.5 $\mu$m
$z$ translation: 2.4 m
rotation about $x,y$-axis: 1.1°
rotation about $z$-axis: 0.01°
rotation quarter wave plate: 1.7°
rotation polariser in front of CCD1: 3.5°

The required accuracy in the normalization factors of the intensity distributions on the CCD-chips are:

normalization factor CCD0 and CCD2: 13%
normalization factor CCD1: 9%

The influence of unequal intensities in the test section and in the reference path on the

average modulus of the phase error is negligible if the quotient of the electric fields is smaller than 1.25.

# References


1. T.A.W.M. Lanen, Digital Holographic Interferometry in Compressible Flow Research, thesis Delft University of Technology, 1992.

2. A.J.P. van Haasteren, Real-time Phase Stepped Speckle Interferometry, thesis Delft University of Technology, 1994.

3. G.E. Sommargren, Up/down frequency shifter for optical heterodyne interferometry. In: Journal of the Optical Society of America, Vol. 65, nr. 8, August 1975.

4. R.N. Shagam and J.C. Wyant, Optical frequency shifter for heterodyne interferometers using multiple rotating polarization retarders. In: Applied Optics, vol. 17, no. 19, 1978.

5. M. Born and E. Wolf, Principles of optics, Pergamon Press, Oxford, 1987.

6. J. Wilson and J.F.B. Hawkes, Optoelectronics An Introduction, 2nd edition, Prentice Hall, London, 1989.

## Series 01: Aerodynamics

01. F. Motallebi, 'Prediction of Mean Flow Data for Adiabatic 2-D Compressible Turbulent Boundary Layers'
1997 / VI + 90 pages / ISBN 90-407-1564-5
02. P.E. Skåre, 'Flow Measurements for an Afterbody in a Vertical Wind Tunnel'
1997 / XIV + 98 pages / ISBN 90-407-1565-3
03. B.W. van Oudheusden, 'Investigation of Large-Amplitude 1-DOF Rotational Galloping'
1998 / IV + 100 pages / ISBN 90-407-1566-1
04. E.M. Houtman / W.J. Bannink / B.H. Timmerman, 'Experimental and Computational Study of a Blunt Cylinder-Flare Model in High Supersonic Flow'
1998 / VIII + 40 pages / ISBN 90-407-1567-X
05. G.J.D. Zondervan, 'A Review of Propeller Modelling Techniques Based on Euler Methods'
1998 / IV + 84 pages / ISBN 90-407-1568-8
06. M.J. Tummers / D.M. Passchier, 'Spectral Analysis of Individual Realization LDA Data'
1998 / VIII + 36 pages / ISBN 90-407-1569-6
07. P.J.J. Moeleker, 'Linear Temporal Stability Analysis'
1998 / VI + 74 pages / ISBN 90-407-1570-X
08. B.W. van Oudheusden, 'Galloping Behaviour of an Aeroelastic Oscillator with Two Degrees of Freedom'
1998 / IV + 128 pages / ISBN 90-407-1571-8
09. R. Mayer, 'Orientation on Quantitative IR-thermografy in Wall-shear Stress Measurements'
1998 / XII + 108 pages / ISBN 90-407-1572-6
10. K.J.A. Westin / R.A.W.M. Henkes, 'Prediction of Bypass Transition with Differential Reynolds Stress Models'
1998 / VI + 78 pages / ISBN 90-407-1573-4
11. J.L.M. Nijholt, 'Design of a Michelson Interferometer for Quantitative Refraction Index Profile Measurements'
1998 / 60 pages / ISBN 90-407-1574-2
12. R.A.W.M. Henkes / J.L. van Ingen, 'Overview of Stability and Transition in External Aerodynamics'
1998 / IV + 48 pages / ISBN 90-407-1575-0
13. R.A.W.M. Henkes, 'Overview of Turbulence Models for External Aerodynamics'
1998 / IV + 40 pages / ISBN 90-407-1576-9

## Series 02: Flight Mechanics

01. E. Obert, 'A Method for the Determination of the Effect of Propeller Slipstream on a Static Longitudinal Stability and Control of Multi-engined Aircraft'
1997 / IV + 276 pages / ISBN 90-407-1577-7
02. C. Bill / F. van Dalen / A. Rothwell, 'Aircraft Design and Analysis System (ADAS)'
1997 / X + 222 pages / ISBN 90-407-1578-5
03. E. Torenbeek, 'Optimum Cruise Performance of Subsonic Transport Aircraft'
1998 / X + 66 pages / ISBN 90-407-1579-3

## Series 03: Control and Simulation

01. J.C. Gibson, 'The Definition, Understanding and Design of Aircraft Handling Qualities'
1997 / X + 162 pages / ISBN 90-407-1580-7
02. E.A. Lomonova, 'A System Look at Electromechanical Actuation for Primary Flight Control'
1997 / XIV + 110 pages / ISBN 90-407-1581-5
03. C.A.A.M. van der Linden, 'DASMAT-Delft University Aircraft Simulation Model and Analysis Tool. A Matlab/Simulink Environment for Flight Dynamics and Control Analysis'
1998 / XII + 220 pages / ISBN 90-407-1582-3

## Series 05: Aerospace Structures and Computional Mechanics

01. A.J. van Eekelen, 'Review and Selection of Methods for Structural Reliability Analysis'
1997 / XIV + 50 pages / ISBN 90-407-1583-1
02. M.E. Heerschap, 'User's Manual for the Computer Program Cufus. Quick Design Procedure for a CUt-out in a FUSelage version 1.0'
1997 / VIII + 144 pages / ISBN 90-407-1584-X
03. C. Wohlever, 'A Preliminary Evaluation of the B2000 Nonlinear Shell Element Q8N.SM'
1998 / IV + 44 pages / ISBN 90-407-1585-8
04. L. Gunawan, 'Imperfections Measurements of a Perfect Shell with Specially Designed Equipment (UNIVIMP)
1998 / VIII + 52 pages / ISBN 90-407-1586-6

## Series 07: Aerospace Materials

01. A. Vašek / J. Schijve, 'Residual Strenght of Cracked 7075 T6 Al-alloy Sheets under High Loading Rates'
1997 / VI + 70 pages / ISBN 90-407-1587-4
02. I. Kunes, 'FEM Modelling of Elastoplastic Stress and Strain Field in Centre-cracked Plate'
1997 / IV + 32 pages / ISBN 90-407-1588-2
03. K. Verolme, 'The Initial Buckling Behavior of Flat and Curved Fiber Metal Laminate Panels'
1998 / VIII + 60 pages / ISBN 90-407-1589-0
04. P.W.C. Provó Kluit, 'A New Method of Impregnating PEI Sheets for the *In-Situ* Foaming of Sandwiches'
1998 / IV + 28 pages / ISBN 90-407-1590-4
05. A. Vlot / T. Soerjanto / I. Yeri / J.A. Schelling, 'Residual Thermal Stresses around Bonded Fibre Metal Laminate Repair Patches on an Aircraft Fuselage'
1998 / IV + 24 pages / ISBN 90-407-1591-2
06. A. Vlot, 'High Strain Rate Tests on Fibre Metal Laminates'
1998 / IV + 44 pages / ISBN 90-407-1592-0
07. S. Fawaz, 'Application of the Virtual Crack Closure Technique to Calculate Stress Intensity Factors for Through Cracks with an Oblique Elliptical Crack Front'
1998 / VIII + 56 pages / ISBN 90-407-1593-9
08. J. Schijve, 'Fatigue Specimens for Sheet and Plate Material'
1998 / VI + 18 pages / ISBN 90-407-1594-7

## Series 08: Astrodynamics and Satellite Systems

01. E. Mooij, 'The Motion of a Vehicle in a Planetary Atmosphere'
1997 / XVI + 156 pages / ISBN 90-407-1595-5
02. G.A. Bartels, 'GPS-Antenna Phase Center Measurements Performed in an Anechoic Chamber'
1997 / X + 70 pages / ISBN 90-407-1596-3
03. E. Mooij, 'Linear Quadratic Regulator Design for an Unpowered, Winged Re-entry Vehicle'
1998 / X + 154 pages / ISBN 90-407-1597-1

3021856

This book describes the theoretical design of a three camera Michelson interferometer set-up for quantitative refractive index measuerments. Although a two camera system is easier to align and less expensive, a three camera interferometer is preferred because the expected measuring accuracy is much better. Here analytical expressions are found for the calculation of the required alignment accuracy of the interferometer's components: three CCD-cameras (six degrees of freedom each), a quarter wave plate (one degree of freedom) and a polariser (one degree of freedom). Also the required accuracy in the normalization of the intensity levels on the CCD-cameras is calculated.

ISBN 90-407-1574-2